traditionally characterized as modeling behaviors associated with schizophrenia. Indeed, mice treated with NMDA receptor antagonist PCP or MK-801, which have been regarded as animal models of schizophrenia, display an increase in both motor activity and sensitivity to psychostimulant (Abi-Saab et al., 1998; Duncan et al., 1999; Ellison, 1995; Javitt and Zukin, 1991; Malhotra et al., 1997).

In this study, we demonstrated that drebrin A knockdown rats display impaired PPI of the acoustic startle response at the stimulation type of PP70. Among a wide available range (65–85 dB) of pre-pulse intensity in acoustic stimulation, the pre-pulse intensity optimal to reveal the dysfunction of sensorimotor gating has been dependent on the types of treatment or disorder (Braff and Geyer, 1990; Braff et al., 2001; Inada et al., 2003). Thus, the present result indicates that the stimulation type of PP70 was more optimal than that of 80 dB for revealing PPI deficit in drebrin A knockdown rats. As shown in Fig. 6, the recovery from the deficit of PPI at PP70 in antisense-treated rats was observed at 18 days after the antisense treatment, when the down-regulated expression of drebrin A protein recovered to the original level. This recovery from the PPI deficit suggests that the disruption of PPI is dependent on the antisense-induced down-regulation of drebrin A in the forebrain such as the neocortex or hippocampus. It has been considered that the PPI reflects the function of the sensorimotor gating system, which partly overlaps with the cognitive function (Bakshi and Geyer, 1998; Braff and Geyer, 1990; Braff et al., 1992; Braff et al., 2001; Geyer, 1998), and that the disruption of PPI provides one of the modeling behaviors observed in schizophrenia, as schizophrenic patients display a significant impairment of PPI (Braff and Geyer, 1990; Braff et al., 1992; Braff et al., 2001; Geyer, 1998; Inada et al., 2003). Recently, it has been reported that an injection of non-competitive NMDA receptor antagonist into the dorsal hippocampus or amygdala produces the disruption of PPI in normal rats, suggesting that hypofunction of excitatory synapses in the multiple limbic regions mediates the PPI deficit (Bakshi and Geyer, 1998). Therefore, it is likely that the PPI deficit found in the drebrin in vivo knockdown rats results from dysfunction of excitatory synapses via antisense-induced modulation of dendritic spine function in the multiple limbic regions, such as the dorsal hippocampus or amygdala.

In the present study, global processes associated with spatial memory were impaired in drebrin A knockdown rats. In the spatial probe test, the preference for the target quadrant was stronger in the Dre-AS rats, suggesting that better memory was acquired by the Dre-AS treatment (see Fig. 7B). However, analysis of the perseverative behavior in the spatial probe test suggested that the stronger preference for the previous target in a novel environment observed in the Dre-AS rats (see Fig. 8) might rather result from a cognitive deficit or worse judgment than better memory, by which these rats are unable to inhibit inappropriate response or inattentive behavior to the sudden disappearance of the target. Another interpretation on the better spatial memory is that the abnormally strong preference for the previous target in the probe test may be due to a deficit in the naturally occurring extinction of memory. However, this interpretation is nearly the same as the cognitive deficit or worse judgment because the extinction of memory will occur when the animal is able to recognize being in any situation different from that memory event. Thus, the "better memory" observed in drebrin knockdown rats should be replaced by the term of "stronger preference" for previous experience due to cognitive deficit leading to perseverative tendencies. This behavioral abnormality in the water-maze resembles the cognitive dysmetria of the schizophrenic symptoms in the inability to receive and process information rapidly that has been associated with dysfunction of prefrontal–thalamic–cerebellar circuitry (Andreasen et al., 1996; Hecker et al., 1998; Wiser et al., 1998).

Because the swimming velocity of the Dre-AS rats in the first session was equal to that of the Dre-RE controls (data not shown), the reduced escape latency observed in the first session in the analysis of spatial memory formation seems to indicate that the drebrin A knockdown rats might have enhanced learning ability (see Fig. 7A). However, since the escape latency in the earliest training session depends largely on an animal's adaptive behaviors in a different situation from the previous event, this behavioral alteration may result from changes in the emotional or cognitive state rather than from increased learning ability. One possible interpretation of the shorter escape latency is also the stronger preference for the previous experience; that is, for the early trials when a maximum of 60 s swim time elapsed, rats were placed on the platform manually for 15 s, in an effort to force them to learn the hidden-platform task. Since most of the rats tested experienced this forced learning at least once, the stronger preference for the previous experience in the Dre-AS rats could make the escape latency shorter in the earlier session.

Due to the coincidence between several abnormal behaviors in drebrin in vivo knockdown rats and schizophrenia-related behaviors in rodents, there has been considerable interest in identifying the relationship between schizophrenic symptoms and dysfunction of excitatory synapses via antisense modulation of the drebrin–mediated dendritic spine function. The brain structures that have been correlated with the positive symptoms of schizophrenia, such as the prefrontal cortex, striatum, thalamus, dorsal hippocampus, or amygdala, largely overlap with the brain regions that have been characterized by high expression of dendritic spine protein drebrin A (see Fig. 1) (Hayashi et al., 1996) and the abundance of spiny neurons. Therefore, the combination of impaired adaptive behaviors, increased sensitivity to psychostimulant, and impaired PPI with stronger preference due to perseverative behavior observed in drebrin in vivo knockdown rats may provide a good animal model of schizophrenia. Further study is needed to demonstrate other schizophrenia-related behaviors, such as behavioral abnormalities in a forced-swim test or the negative symptoms of defective social interaction.

Acknowledgements

This study was supported by the Health Science Research Grants (no. H12-brain-018) from the Ministry of Health, Labor and Welfare, Japan. This investigation was also supported in part by the Grant for Scientific Research from Kitasato University Graduate School of Medical Science, Japan. We would like to thank Mr. Sakaguchi of Kitasato University for his kind help in the data analysis of water-maze test.

References

Abi-Saab, W.M., D'Souza, D.C., Moghaddam, B., Krystal, J.H., 1998. The NMDA antagonist model or schizophrenia: promise and pitfalls. Pharmacopsychiatry 31 (Suppl 2), 104–109.

Amara, S.G., Kuhar, M.J., 1993. Neurotransmitter transporters: recent progress. Annu. Rev. Neurosci. 16, 73–93.

Andreasen, N.C., O'Learly, D.S., Cizadlo, T., Arndt, S., Rezai, K., Ponto, L.L., Watkins, G.L., Hichwa, R.D., 1996. Schizophrenia and cognitive dysmetria: a positron-emission tomography study of dysfunctional prefrontal–thalamic–cerebellar circuitry. Proc. Natl. Acad. Sci. U.S.A. 93, 9985–9990.

Bakshi, V.P., Geyer, M.A., 1998. Multiple limbic regions mediate the disruption of prepulse inhibition produced in rats by the noncompetitive NMDA antagonist dizocilpine. J. Neurosci. 18, 8394–8401.

Braff, D.L., Geyer, M.A., 1990. Sensorimotor gating and schizophrenia: human and animal model studies. Arch. Gen. Psychiatry 47, 181–188.

Braff, D.L., Grillon, C., Geyer, M.A., 1992. Gating and habituation of the startle reflex in schizophrenic patients. Arch. Gen. Psychiatry 49, 206–215.

Braff, D.L., Geyer, M.A., Light, G.A., Sprock, J., Perry, W., Cadenhead, K.S., Swerdlow, N.R., 2001. Impact of prepulse characteristics on the detection of sensorimotor gating deficits in schizophrenia. Schizophr. Res. 49, 171–178.

Carlsson, M., Carlsson, A., 1990. Interaction between glutamatergic and monoaminergic systems within the basal ganglia: implications for schizophrenia and Parkinson's disease. Trends Neurosci. 13, 272–276.

Corbett, R., Camacho, F., Woods, A.T., Kerman, L.L., Fishkin, R.J., Brooks, K., Dunn, R.W., 1995. Antisychotic agents antagonize non-competitive *N*-methyl-D-aspartate antagonist-induced behaviors. Psychopharmacology (Berlin) 120, 67–74.

Duncan, G.E., Zorn, S., Lieberman, J.A., 1999. Mechanisms of typical and atypical antipsychotic drug action in relation to dopamine and NMDA receptor hypofunction hypotheses of schizophrenia. Mol. Psychiatry 4, 418–428.

Ellison, G., 1995. The *N*-methyl-D-aspartate antagonists phencyclidine, ketamine, dizoclipine as both behavioral and anatomical models of the dementias. Brain Res. Brain Res. Rev. 20, 250–267.

Engert, F., Bonhoeffer, T., 1999. Dendritic spine changes associated with hippocampal long-term synaptic plasticity. Nature 399, 66–70.

Geyer, M.A., 1998. Behavioral studies of hallucinohenic drugs in animals: implications for schizophrenia research, Pharmacopsychiatry Suppl. 2, 73–79.

Giros, B., Jaber, M., Jones, S.R., Wightman, R.M., Caron, M.G., 1996. Hyperlocomotion and indifference to cocaine and amphetamine in mice lacking the dopamine transporter. Nature 379, 606–612.

Harigaya, Y., Shoji, M., Shirao, T., Hirai, S., 1996. Disappearance of actin-binding protein drebrin, from hippocampal synapses in Alzheimer's disease. J. Neurosci. Res. 43, 87–92.

Hatanpaa, K., Isaacs, K.R., Shirao, T., Brady, D.R., Rapoport, S.I., 1999. Loss of proteins regulating synaptic plasticity in normal aging of the human brain and in Alzheimer disease. J. Neuropathol. Exp. Neurol. 58, 637–643.

Hayashi, K., Ishikawa, R., Ye, L.H., Takata, K., Kohama, K., Shirao, T., 1996. Modulatory role of drebrin in the cytoskeleton within dendritic spines in the rat cerebral cortex. J. Neurosci. 16, 7161–7170.

Hayashi, K., Shirao, T., 1999. Change in the shape of dendritic spines caused by overexpression of drebrin in cultured cortical neurons. J. Neurosci. 19, 3918–3925.

Hecker, S., Rauch, S.L., Goff, D., Savage, C.R., Schacter, D.L., Fischman, A.J., Alpert, N.M., 1998. Impaired recruitment of the hippocampus during conscious recollection in schizophrenia. Nat. Neurosci. 1, 318–322.

Inada, K., Ishigooka, J., Anzai, T., Suzuki, E., Miyaoka, H., Saji, M., 2003. Antisense hippocampal knockdown of NMDA-NR1 by HVJ-liposome vector induces deficit of prepulse inhibition but not of spatial memory. Neurosci. Res. 45, 473–481.

Iwakuma, M., Anzai, T., Kobayashi, S., Ogata, M., Kaneda, Y., Ohno, K., Saji, M., 2003. Antisense in vivo knockdown of synaptotagmin I and synapsin I by HVJ-liposome mediated gene transfer modulates ischemic injury of hippocampus in opposing ways. Neurosci. Res. 45, 285–296.

Javitt, D.C., Zukin, S.R., 1991. Recent advances in the phencyclidine model of Schizophrenia. Am. J. Psychiatry 148, 1301–1308.

Kaneda, Y., 1999. Development of a novel fusogenic viral liposome system (HVJ-liposomes) and its applications to the treament of acquired diseases. Mol. Memb. Biol. 16, 119–122.

Keller, A., 2002. Use-dependent inhibition of dendritic spines. Trends Neurosci. 25, 541–544.

Kobayashi, S., Ohno, K., Iwakuma, M., Kaneda, Y., Saji, M., 2002. Synaptotagmin I hypothalamic knockdown prevents amygdaloid seizure-induced damage of hippocampal neurons but not of entorhinal neurons. Neurosci. Res. 44, 455–465.

Lendvai, B., Stern, E.A., Chen, B., Svoboda, K., 2000. Experience-dependent plasticity of dendritic spines in the developing rat barrel cortex in vivo. Nature 404, 876–881.

Malhotra, A.K., Pinals, D.A., Adler, C.M., Elman, I., Clifton, A., Pickar, D., Breier, A., 1997. Ketamine-induced exacerbation of psychotic symptoms and cognitive impairment in neuoleptic-free schizophrenics. Neuropsychopharmacology 17, 141–150.

Marrs, G.S., Steven, H.G., Dailey, M.E., 2001. Rapid formation and remodeling of postsynaptic dendrites in developing dendrites. Nat. Neurosci. 4, 1006–1013.

Morris, R.G., Garrud, P., Rawlins, J.N.P., O'Keef, J., 1982. Place navigation impaired in rats with hippocampal lesions. Nature 297, 681–683.

Okabe, S., Miwa, A., Okado, H., 2001. Spine formation and correlated assembly of presynaptic and postsynaptic molecules. J. Neurosci. 21, 6105–6114.

Saeki, Y., Matsumoto, N., Nakano, Y., Mori, M., Awai, K., Kaneda, Y., 1997. Development and characterization of cationic liposomes conjugated with HVJ (Sendai virus): reciprocal effect of cationic lipid for in vitro and in vivo gene transfer. Hum. Gene Ther. 8, 2133–2144.

Shim, K.S., Lubec, G., 2002. Drebrin, a dendritic spine protein, is manifold decreased in brains of patients with Alzheimer's disease and Down syndrome. Neurosci. Lett. 324, 209–212.

Shirao, T., Obata, K., 1986. Immunochemical homology of 3 developmentally regulated brain proteins and their developmental change in neuronal distribution. Brain Res. 394, 233–244.

Shirao, T., Inoue, H.K., Kano, Y., Obata, K., 1987. Localization of a developmentally regulated neuron-specific protein S54 in dendrites as revealed by immunoelectron microscopy. Brain Res. 413, 374–378.

Shirao, T., Hayashi, K., Ishikawa, R., Isa, K., Asada, H., Ikeda, K., Uyemura, K., 1994. Formation of thick curving bundles of actin by drebrin A expressed in fibroblasts. Exp. Cell Res. 215, 145–153.

Shirao, T., 1995. The roles of microfilament-associated proteins, drebrins, in brain morphogenesis: a review. J. Biochem. (Tokyo) 117, 231–236.

Shirao, T., Sekino, Y., 2001. Clustering and anchoring mechanisms of molecular constituents of postsynaptic scaffolds in dendritic spines. Neurosci. Res. 40, 1–7.

Takahashi, H., Sekino, Y., Tanaka, S., Mizui, T., Kishi, S., Shirao, T., 2003. Drebrin-dependent actin clustering in dendritic filopodia governs synaptic targeting of postsynaptic density-95 and dendritic spine morphogenesis. J. Neurosci. 23, 6586–6595.

Tanaka S., Sekino Y., Shirao, T., 2001. Change of dendritic spine length induced by drebrin A knockdown using antisense oligonucleotides in vitro. Soc. Neurosci. Abstr. 29.

Wiser, A.K., Andreasen, N.C., O'Learly, D.S., Watkins, G.L., Boles Ponto, L.L., Hichwa, R.D., 1998. Dysfunctional cortico-cerebellur circuits cause 'cognitive dysmetria' in schizophrenia. Neuroreport 9, 1895–1899.

Yamada, K., Moriguchi, A., Morishita, R., Aoki, M., Mikami, H., Oshima, T., Ninomiya, M., Kaneda, Y., Higaki, J., Ogihara, T., 1996. Efficient oligonucleotide delivery using the HVJ-liposome method in the central nervous system. Am. J. Physiol. 271, R1212–R1220.

Zapata, A., Capdevilla, J.L., Tarrason, G., Martinez, J.M., Piulats, J., Trulla, R., 1997. Effects of NMDA-R1 antisense oligonucleotides administration: behavioral and radioligand binding studies. Brain Res. 745, 114–120.

Current Biology, Vol. 14, 650–658, April 20, 2004, ©2004 Elsevier Ltd. All rights reserved. DOI 10.1016/j.cub.2004.03.063

Drebrin Is a Novel Connexin-43 Binding Partner that Links Gap Junctions to the Submembrane Cytoskeleton

Eugenia Butkevich,[1,2] Swen Hülsmann,[1,2] Dirk Wenzel,[3] Tomoaki Shirao,[4] Rainer Duden,[5,*] and Irina Majoul[3,5,*]
[1]Department of Neurophysiology
University of Göttingen
Germany
[2]Research Centre Molecular Physiology of the Brain
Göttingen
Germany
[3]Department of Neurobiology
Max-Planck-Institute for Biophysical Chemistry
Göttingen
Germany
[4]Department of Neurobiology and Behavior
Gunma University Graduate School of Medicine
Maebashi
Japan
[5]Cambridge Institute for Medical Research
University of Cambridge
Cambridge
United Kingdom

Summary

Background: Connexins form gap junctions that mediate the transfer of ions, metabolites, and second messengers between contacting cells. Many aspects of connexin function, for example cellular transport, plaque assembly and stability, and channel conductivity, are finely tuned and likely involve proteins that bind to connexins' cytoplasmic domains. However, little is known about such regulatory proteins. To identify novel proteins that interact with the COOH-terminal domain of Connexin-43 (Cx43), the most widely expressed connexin family member, we applied a proteomics approach to screen fractions of mouse tissue homogenates for binding partners.

Results: Drebrin was recovered as a binding partner of the Cx43 COOH-terminal domain from mouse brain homogenate. Drebrin had previously been described as an actin binding protein that diminishes in brains during Alzheimer's disease. The novel Drebrin-Cx43 interaction identified by proteomics was confirmed by colocalization of endogenous proteins in astrocytes and Vero cells, coimmunoprecipitation, electron microscopy, electrophysiology, coexpression of both proteins with fluorescent tags, and live-cell FRET analysis. Depletion of Drebrin in cells with siRNA results in impaired cell-cell coupling, internalization of gap junctions, and targeting of Cx43 to a degradative pathway.

Conclusions: We conclude that Drebrin is required for maintaining Cx43-containing gap junctions in their functional state at the plasma membrane. It is thus possible that Drebrin may interact with gap junctions in zones of cell-cell contacts in a regulated fashion in response to extracellular signals. The rearrangement or disruption of interactions between connexins and the Drebrin-containing submembrane cytoskeleton directs connexins to degradative cellular pathways.

*Correspondence: im266@cam.ac.uk (I.M.), rd217@cam.ac.uk (R.D.)

Introduction

Gap junctions are transmembrane channels between contacting cells and mediate intercellular communication and signaling by permitting the passage of ions, metabolites, and second messengers [1–3]. Connexins organize themselves into hexameric assemblies, named hemi-channels or connexons, that contain six subunits. After transport to the plasma membrane, connexons can align between neighboring cells head-to-head to form the functional and regulated gap junction channels. More than 20 connexin isoforms encoded by different genes have been described in the human genome [4], allowing the synthesis of a large number of channels with different functional properties. All connexins comprise four transmembrane helices, two extracellular loops rigidly held together by disulfide linkages, and three variable cytoplasmic domains: amino terminus, cytoplasmic loop, and carboxy terminus [1]. The importance of gap junctions for multicellular organisms is highlighted by a wide array of different human diseases and mouse phenotypes that arise from defects in these genes. In mice null mutations in Cx43, the main connexin of gap junctions in heart and many other tissues, cause death shortly after birth. The hearts of such mice beat, but a malformation of their heart is fatal. In humans, the inherited defects in individual connexin isoforms are associated with demyelinating disorders of the peripheral nervous system, severe hearing impairment, eye lens cataracts, skin disorders, heart arrhythmias, and heart malformation [4]. Some of these diseases have a significant impact on the human population, with Cx26 mutations accounting for more than 50% of the cases of inherited asyndromic sensorineural deafness [4]. The intracellular transport of connexins, connexon assembly and channel formation, gap junction plaque assembly at the plasma membrane, and modulation of channel activities are most likely governed by interactions with regulatory and structural proteins that recognize specific sequence motifs in the cytoplasmic domains of connexins. However, only a few such connexin-interacting proteins have been described to date, and these include the tight junction protein ZO-1, tubulin, and the kinase c-Src [5–8].

In this study we screened for new interaction partners of Cx43, the most widely expressed member of the connexin family. We identified Drebrin as a novel interaction partner of the Cx43 COOH-terminal domain at the plasma membrane. Drebrin, previously described as an actin binding protein [9], was recovered from mouse brain homogenates. We confirmed the importance of Cx43/Drebrin interaction in living cells and analyzed the effects of RNAi depletion of Drebrin on gap junction

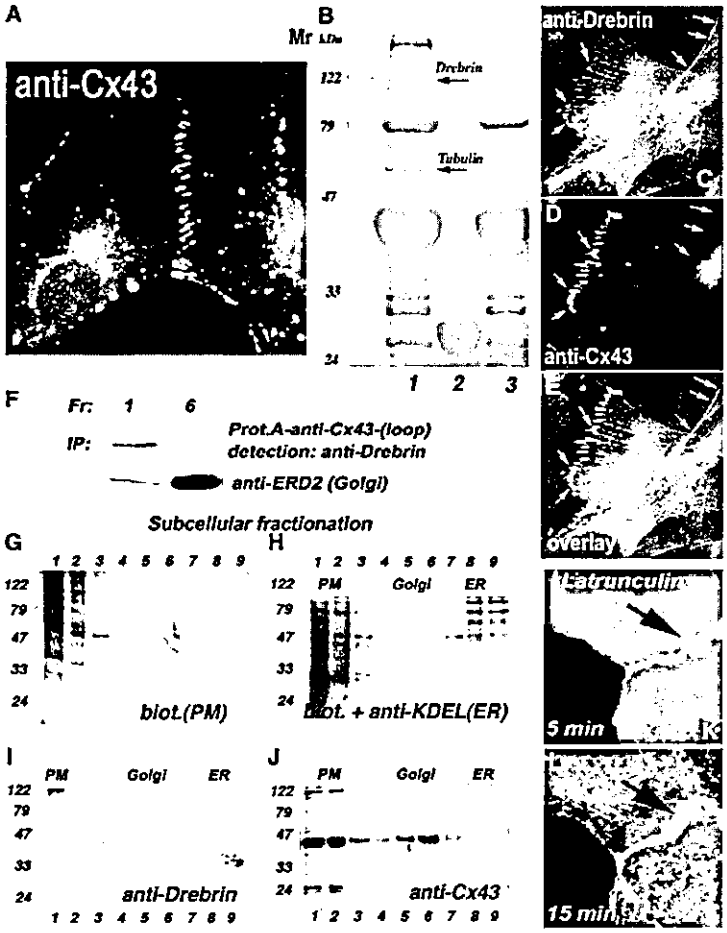

Figure 1. Drebrin Interacts with Connexin-43 In Vitro and Colocalizes with Connexin-43 at the Plasma Membrane by Immunofluorescence

(A) Distribution of endogenous connexin-43 in astrocytes.

(B) SDS-PAGE and Coomassie staining of proteins obtained in a pull-down assay with a GST-fusion protein encompassing the Cx43-COOH-terminal domain (residues 234–382) with a membrane fraction of mouse brain homogenate. Arrows indicate the positions of Drebrin and tubulin. Both proteins were identified by MALDI-Q-TOF in the pull-down fraction.

(C–E) Plasma membrane colocalization of endogenous Drebrin E and Cx43 in astrocytes as detected with anti-Cx43 and anti-Drebrin M2F6 antibodies, respectively. In the noncontacting regions of the plasma membrane, Drebrin E does not colocalize with Cx43.

(F–J) Subcellular fractionation of Vero cells and characterization of the separated fractions. (F) anti-Cx43 antibodies (raised against the first extracellular loop) immobilized on protein A Sepharose can coimmunoprecipitate Drebrin from the plasma membrane fraction (1). Anti-ERD2 antibodies (used as a control of the Golgi fractions) show the relative distribution of transmembrane Golgi protein in fractions 1 and 6. (G) Fractions containing biotinylated proteins, corresponding to the plasma membrane (PM), were detected with streptavidin-peroxidase. (H) A blot probed with streptavidin-peroxidase (fractions 1–3) was again exposed to anti-KDEL antibodies to reveal the ER (fractions 8 and 9). (I) Drebrin was detected in the pellet of the plasma membrane fraction. (J) Cx43 was present in both plasma membrane and the Golgi fractions.

(K and L) Time-dependent accumulation of Drebrin under the plasma membrane of Vero cells transfected with CFP-Drebrin and Cx43-YFP upon Latrunculin B treatment.

stability and permeability. Our data indicate that Drebrin is required to maintain functional Cx43-containing gap junctions at the cell surface.

Results and Discussion

Pull-Down Assays with the Cx43 COOH-Terminal Domain Recover Drebrin from Brain Homogenate

In search of new interaction partners of Cx43, we used a proteomics approach to screen subcellular fractions from different mouse tissues (brain, kidney, lung, heart, and liver) for proteins that may interact with a GST-fusion protein encompassing the Cx43 COOH-terminal domain (residues 234–382), which is normally exposed to the cytosol. Pull-down assays with this Cx43-COOH terminal domain fusion protein recovered several bands that were resolved by SDS-PAGE and visualized with Coomassie Blue (Figure 1B). MALDI/Q-TOF (matrix-assisted laser desorption ionization/quadrupole time-of-flight) mass spectrometry analysis of tryptic peptides identified a number of these proteins. One of them, Drebrin E, was reproducibly recovered in pull-down assays from the brain membrane fraction via the Cx43-GST fusion protein (Figure 1B). Drebrin has been previously described as an actin binding protein [9] whose level is greatly decreased in brains of Alzheimer patients [10]. We obtained 22 peptides by Q-TOF sequence analysis with exact matches to the cDNA-derived protein sequence of Drebrin ($p < 0,05$) (see Table S1 in the Supplemental Data available with this article online).

Another band obtained in the pull-down assay was identified by MALDI Q-TOF analysis as β-tubulin (see arrow in Figure 1B; peptide data not shown), which has already been described as an interaction protein for Cx43 [7]. A further previously described Cx43 binding partner, the tight-junction protein ZO-1 [5, 6], was present in the starting plasma membrane fractions, as detected by immunoblots with a ZO-1 antibody. Nevertheless, ZO-1 was not recovered on the Cx43-GST fusion protein under our experimental conditions, which included the presence of 1% Triton and ATP in the binding reactions and wash buffer.

Next we analyzed the distribution of endogenous Drebrin E and Cx43 by immunofluorescence with the corresponding antibodies. In astrocytes (Figures 1C–1E) and Vero cells (Figures 3A and 3B), a clear colocalization of

both proteins underneath the plasma membrane in the region of cell-cell contacts was observed. On the other hand, inside the cell and in noncontacting regions of the plasma membrane, Drebrin E did not colocalize with Cx43 (Figures 1C–1E, 3A, and 3B).

Subcellular fractionation of Vero cells, performed as we described previously [11] and in the Supplemental Data available with this paper online, revealed that Cx43 was present in both the plasma membrane (PM) and Golgi fractions (Figure 1J), whereas Drebrin was detected only in the plasma membrane fraction (Figure 1I). Fractions containing Golgi membranes were detected by an enzyme assay for UDP-galactosyltransferase, and the plasma membrane fractions were recognized by streptavidin-peroxidase after cell-surface biotinylation of intact cells on ice (Figure 1G), as described by us previously [11]. Golgi fractions in the gradient were detected with antibodies against the transmembrane Golgi KDEL-receptor (ERD2). ER fractions were recognized by the maximal activity of Rotenone-insensitive cytochrome-C reductase [11] in gradient fractions and with antibodies directed against the KDEL-peptide sequence (which is characteristic for many ER resident lumenal proteins) in immunoblots (Figure 1H; fractions 8 and 9). Immunoprecipitations with anti-Cx43 antibodies (raised against the first external loop, residues 46–68) were performed from the fractions, and immunoblotting with anti-Drebrin antibodies allowed analysis of coprecipitating proteins. Drebrin was immunoprecipitated from the PM fraction but not from the Golgi fractions (Figure 1F). These results confirm that Drebrin is associated with Cx43 in the plasma membrane fraction.

To test whether the submembrane localization of Drebrin depends on the presence of polymerized actin, we treated Vero cells with the actin-depolymerizing drug Latrunculin B (100 nM). In Vero cells transfected with CFP-Drebrin and Cx43-YFP, Drebrin was still detected underneath the PM of contacting cells after Latrunculin B treatment and thus was not dispersed through the cytoplasm in the absence of actin filaments (Figures 1K and 1L).

Live-Cell Analyses Reveal Drebrin/Cx43 Interactions in Submembrane Regions of Cell-Cell Contacts

Live-cell imaging of COS cells expressing CFP-Drebrin and Cx43-YFP revealed that Drebrin strongly accumulates in contacting regions of the plasma membranes only when Cx43 is present there (Figure 2A–2C). To confirm the close molecular proximity of Drebrin and Cx43 in the regions of cell-cell contacts, we used live-cell fluorescence resonance energy transfer (FRET) and an acceptor bleach protocol that we had developed earlier [12, 13]. For these experiments, CFP-Drebrin and Cx43-YFP were coexpressed in Vero cells. In case of FRET proximity, the photoinactivation of the acceptor (Cx43-YFP) results in an increase of the fluorescence of the donor (CFP-Drebrin). First, donor and acceptor images were acquired as follows: donor before bleach (Dbb) and acceptor before bleach (Abb) (Figures 2D and 2E). Photoinactivation of the acceptor (Cx43-YFP) was performed with an external laser at λ_{ex} 530 nm, and images were acquired as follows: acceptor after bleach (Aab) and donor after bleach (Dab). In the regions of cell-cell contacts containing CFP-Drebrin and Cx43-YFP, a clear FRET signal was revealed by an increase in the donor fluorescence (CFP-Drebrin) after the acceptor (Cx43-YFP) was photoinactivated (Figures 2F and 2G).

For a more precise characterization of the CFP-Drebrin/Cx43-YFP interaction underneath the plasma membrane, we analyzed the comparative degree of the donor dequenching along the interface of contacting cells upon direct photoinactivation of the acceptor (Cx43-YFP) by using image data processing with the MetaMorph 6.0 program (Figure 2H). The comparison of two graphs derived from the same cellular region obtained before (Dbb) and after (Dab) acceptor inactivation revealed a 15%–25% increase in the donor fluorescence (small arrows in zones of cell-cell contacts in Figure 2H). As a negative control, the unchanged background region of the same cell is depicted before and after the acceptor bleach (big arrows in Dbb and Dab, Figure 2H). The degree of acceptor photoinactivation in each pixel along the linescan is shown in Figure 2H (Abb, Aab). 3D reconstruction of the profile scan revealed the distribution of FRET between CFP-Drebrin and Cx43-YFP underneath the plasma membrane (Figure 2I).

We further confirmed FRET proximity between CFP-Drebrin and Cx43-YFP by using a Zeiss LSM 510 META microscope setup. CFP-Drebrin and Cx43-YFP interactions were analyzed in living cells during the time-dependent photoinactivation of the acceptor in the region of cell-cell contacts where both donor and acceptor were present (Figure 2J). The time-dependent increase in the donor fluorescence (CFP-Drebrin) was inversely proportional to the degree of acceptor (Cx43-YFP) inactivation (Figure 2K). All images are representative of at least three independent sets of experiments and confirm that the interaction between Drebrin E and Cx43 occurs in the region of cell-cell contact in a living cell.

Disruption of Drebrin/Cx43 Interactions by Drebrin RNAi Directs Cx43 for Degradation

To better understand the functional importance of the Drebrin/Cx43 interaction in a live cell, we decreased the level of Drebrin in Vero cells by using transfection with siRNA duplex oligos directed against Drebrin (see Experimental Procedures and [14]). In control cells, Drebrin E and Cx43 were colocalized in the regions of cell-cell contact by immunofluorescence (Figures 3A and 3B). Forty-eight hours after oligofectamine transfection with the siRNA oligos against Drebrin, we observed a significant decrease in both the immunoblot (Figure 3M) and immunofluorescence signals with anti-Drebrin antibodies (compare Figures 3A and 3D). Drebrin siRNA-silenced cells showed a strong decrease of the staining for Cx43 (Figure 3E). In control Vero cells transfected with Cx43-GFP, immunoelectron microscopy with antibodies against Drebrin or Cx43 revealed that both proteins are present in plasma membrane regions containing gap junctions (Figure 3C). We observed that transfection with Drebrin siRNA induced the scattering of Cx43-GFP through the cytoplasm (Figure 3G). Immunoelectron microscopy analysis of Vero cells transfected with Drebrin

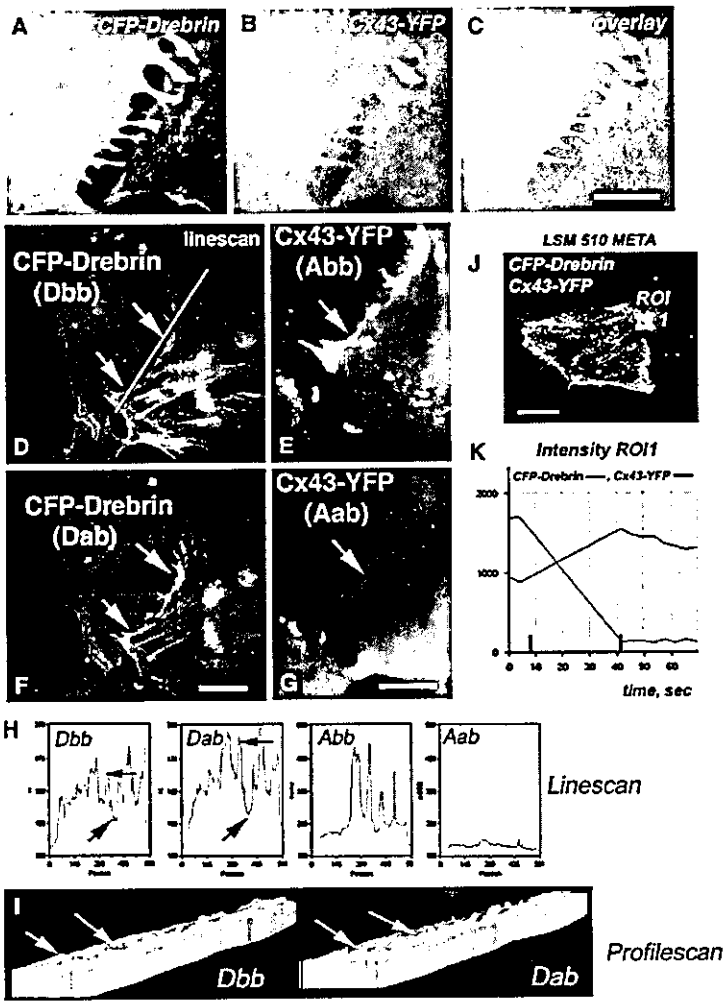

Figure 2. CFP-Drebrin and Cx43-YFP Colocalize in Living Cells and Show a FRET Interaction

(A–C) COS cells transfected with CFP-Drebrin and Cx43-YFP reveal strong colocalization of both proteins in the regions of cell-cell contacts. Note that CFP-Drebrin also accumulates in regions of cell-cell contact where Cx43-YFP is present.

(D–K) FRET analyses of live Vero cells expressing CFP-Drebrin/Cx43-YFP. (D and E) Donor (Dbb) and acceptor (Abb) images before acceptor inactivation. (F and G) Donor (Dab) and acceptor (Aab) images after acceptor photoinactivation done with an external laser at λ_{ex} 530 nm. (H) corresponding linescans (Dbb, Dab, Abb, Aab) along the cell-cell interface; small arrows indicate an increase in donor fluorescence, and big arrows show the unchanged background. (I) 3D reconstruction of a profile scan shows the distribution of FRET between CFP-Drebrin and Cx43-YFP under the plasma membrane (compare Dab to Dbb). (J and K): FRET between CFP-Drebrin and Cx43-YFP detected with the LSM 510 META microscope setup. The diagram shows that the time-dependent increase in donor fluorescence (CFP-Drebrin, green) is inversely proportional to the degree of acceptor (Cx43-YFP, red) inactivation (K).

siRNA revealed the presence of Cx43 in multivesicular intracellular membrane structures inside the cell (Figure 3F), most likely indicating that this connexon material had undergone internalization and was subject to degradation. This contrasts with a prominent cell-cell contact pattern observed in control cells (Figure 3C). Microinjection of calcein into Vero cells transfected with Drebrin siRNA resulted in a decreased ability to transfer dye to the neighboring cells as compared to the control cells (Figure 3K and 3L).

The results show that in Drebrin siRNA transfected cells the connexons are not able to maintain functional gap junctions, resulting in a decreased transfer of calcein to the surrounding cells. The decrease in the endogenous Drebrin level in siRNA-transfected Vero cells also resulted in a dramatic decrease of the endogenous Cx43 level compared to that of the control cells (Figure 3M); this decrease correlates well with the disappearance of Cx43 from the submembrane zones of cell-cell contacts. Furthermore, in actin-GFP-expressing cells we observed extensive ruffling of the plasma membrane after transfection with Drebrin siRNA that was not observed in control cells (Figures 3I and 3J).

Functional Stabilization of Gap Junctions In Astrocytes on the Plasma Membrane by Drebrin May Favor Increased Cell-Cell Coupling and Dye Transfer

We examined the cell-cell coupling in astrocytes and Vero cells by using electrophysiology and dye transfer. Compared to Vero cells (Figure 4B), astrocytes showed strong cell coupling (Figure 4A). We compared the localization of endogenous Cx43 and Drebrin in both cell types by immunofluorescence with anti-Cx43 and anti-Drebrin antibodies. Astrocytes showed strong staining of the plasma membrane for Cx43 (Figure 4C, see also Figures 1C and 1D). In Vero cells endogenous Cx43 showed weaker staining of the plasma membrane and pronounced labeling of the Golgi region (Figure 4D). Plasma membrane localization of Cx43 in astrocytes (Figure 4C) correlates with stronger electrical coupling (Figure 4A) compared to that in Vero cells (Figure 4B). Cx43-GFP transfected into Vero cells localizes to the cell-cell interfaces (Figure 4B, upper right panel) and favors increased cell-cell coupling (data not shown). Cotransfection of Vero cells with Cx43-GFP and siRNA against Drebrin prevented the appearance of Cx43-GFP

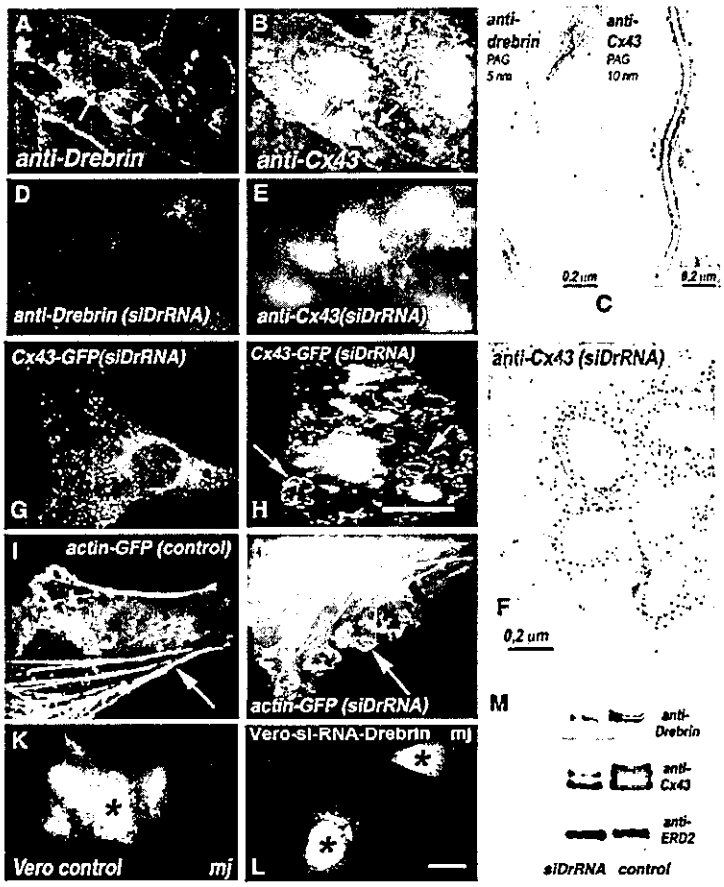

Figure 3. Cx43 in Cells Treated with Drebrin siRNA

(A and B) Distribution of endogenous Drebrin and Cx43 in Vero cells as revealed by immunofluorescence with anti-Drebrin and anti-Cx43 antibodies. Both proteins colocalize under the plasma membrane but do not colocalize in the Golgi region (see the arrows).

(C) The distribution of CFP-Drebrin and Cx43-YFP in Vero cells as detected by immunoelectron microscopy. Note that in Vero cells (which do not have tight junctions, desmosomes, or adherens junctions) Drebrin is present in regions of cell-cell contact with a gap junction appearance.

(D and E) Localization of Drebrin and Cx43 detected 48 hr after transfection of Vero cells with siRNA against Drebrin; the same antibodies as in (A) and (B) were used for detection. Note that the decrease in the level of Drebrin correlates with the decrease of Cx43 immunoreactivity and disappearance of Cx43 from the submembrane zones of cell-cell contacts.

(F) Formation of Cx43-GFP-containing multimembrane clusters in Vero cells cotransfected with siRNA against Drebrin (16 hr) was detected by immunoelectron microscopy with anti-GFP antibody.

(G) Scattering of Cx43-GFP through the cytoplasm in Vero cells transfected first with siRNA against Drebrin (24 hr) and then by Cx43-GFP transfection (10 hr).

(H) Vero cells cotransfected with siRNA against Drebrin and Cx43-GFP (10 hr).

(I and J) Vero cells transfected with GFP-Actin (I) or cotransfected with siRNA directed against Drebrin and GFP-Actin (J). The absence of Drebrin also induces ruffling of the plasma membrane (shown at 10 hr after transfection).

(K and L) Calcein transfer between control (K) and siRNA-Drebrin-transfected (l) cells 20 min after microinjection.

(M) Immunoblot analysis of Vero cells transfected with siRNA against Drebrin. Note that the decrease in Drebrin level results in a dramatic reduction of the level of Cx43 compared to that in control cells. Anti-ERD2 antibodies were used as a loading control.

in regions of cell-cell interfaces. Instead, Cx43-GFP staining was detected throughout the cytoplasm in small punctate structures and in a perinuclear region (Figure 4B, lower right panel).

We used double whole-cell voltage clamp recordings of a pair of primary cultured mouse astrocytes to analyze the state of cell-cell contact permeability (Figure 4E). One cell of the pair was exposed to voltage pulses of 200 ms with a holding potential at −70 mV in 10 mV increments (cell 1), whereas the adjacent cell was kept at −70 mV (cell 2). Current responses from both cells, i.e., the stimulated cell (I_1) and the neighboring cell coupled through the gap junctions (I_2) to the first cell, were recorded.

Comparison of the currents that pass through the gap junctions (I_2) of control cells, of cells cotransfected with Drebrin siRNA and a plasmid encoding the transmembrane Golgi protein p23-CFP, or of control cells transfected with just the p23-CFP plasmid revealed a strong decrease in cell-cell permeability in Drebrin siRNA-transfected astrocytes (Figure 4E). The fact that this effect was reproducible indicates that siRNA-mediated depletion of Drebrin strongly decreases cell-cell permeability, an observation that was confirmed by stastistical evaluation (n = 6 for control cells and n = 5 for cells transfected with Drebrin siRNA) (Figure 4E, right panel). After siRNA-mediated depletion of Drebrin, calcein transfer between astrocytes (Figures 4G and 4H) was also strongly decreased from that in control astrocytes (Figure 4F), although the overall level of dye transfer even in Drebrin-depleted astrocytes still remained higher than in Vero control cells (data not shown).

Cx43 is a protein that is known to be phosphorylated on both serine and tyrosine residues, which changes its mobility upon SDS-PAGE [15, 16, 17]. Normally, in immunoblots of cultured mouse astrocytes, the anti-Cx43 antibodies show predominantly the upper, phosphorylated bands of Cx43 (Figure 4C, lower panel), and in Vero cells they show predominantly the lower, nonphosphorylated band (Figure 4D, lower panel). After partial depletion of Drebrin in cultured astrocytes by Drebrin siRNA, we detected fewer of the phosphorylated upper bands of Cx43 with anti-Cx43 antibodies (Figure 4C, lower panel). The functional consequences of Cx43 phosphorylation have been widely debated [15, 16].

Recently, Faucheux and coworkers, using inhibitors

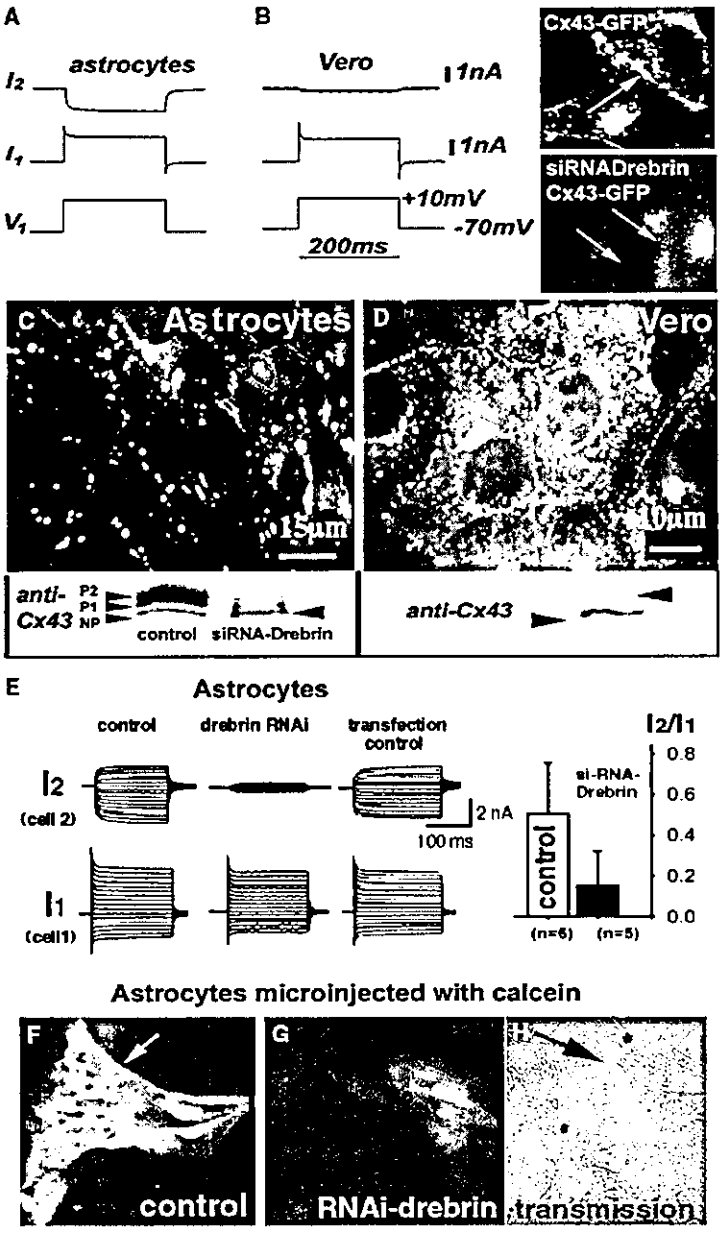

Figure 4. Drebrin Depletion by siRNA in Astrocytes Results in Reduced Electrical Coupling and Reduced Dye Transfer and Correlates with Loss of Cx43 Phosphorylated Bands

(A and B) A voltage step from −160 to +10 mV was applied to cell 1 while its contacting cell, cell 2, was kept at −70 mV. Current responses from stimulated cell 1 (I1) and from the neighboring cell 2 (I2) were recorded. Note that current response in astrocytes is always stronger than in Vero cells. Right: Vero cells transfected with Cx43-GFP and Cx43-GFP/siRNA Drebrin. Note that depletion of Drebrin facilitates the removal of connexins from the plasma membrane ([B], right panel) and thus decreases cell-cell coupling.

(C and D) Astrocytes and Vero cells reveal different cellular distribution of endogenous Cx43. Strong staining of the plasma membrane can be seen in astrocytes, whereas in Vero cells endogenous Cx43 showed only a punctate staining of the plasma membrane and a distinct labeling of Golgi membranes. Immunoblot with anti-Cx43 antibodies shows predominantly the phosphorylated upper bands of Cx43 in astrocytes and predominantly nonphosphorylated lower bands in Vero cells. After partial depletion of Drebrin in cultured astrocytes with siRNA, fewer upper phosphorylated bands of P1 and P2 of Cx43 can be detected.

(E) Double whole-cell voltage clamp recordings of a pair of primary-culture mouse astrocytes. Currents from the stimulated cell (I1) and currents that pass through the gap junctions (I2) were recorded from control cells, cells cotransfected with siRNA against Drebrin plus a control plasmid encoding the transmembrane Golgi protein p23-CFP, or cells transfected with the p23-CFP plasmid alone [11]. One cell of the pair was exposed to voltage pulses of 200 ms with a holding potential of −70 mV in 10 mV increments (cell 1), and the adjacent cell was kept at −70 mV (cell 2). Cells transfected with siRNA against Drebrin were recognized by the p23-CFP signal and by Cy-3 label of the oligos. Three representative cells are shown together with a statistical evaluation (n = 5 for control cells and n = 6 for cells transfected with Drebrin siRNA). Control astrocytes: I2/I1 = 0.517 ± 0.27 (n = 6); RNAi Drebrin: I2/I1 = 0.14 ± 0.03 (n = 5), p = 0.004.

(F) Astrocytes microinjected with calcein display the transfer of dye to the adjacent cells within seconds via the functional gap junctions.

(G and H) There is a strong decrease in calcein transfer observed in astrocytes transfected with Drebrin siRNA (G), although contacting cells are clearly visible in the transmission light image.

of cAMP protein kinase (PKA) and protein kinase C (GF109203X), showed a correlation between disappearance of Cx43 phosphorylated bands and a strong decrease in gap-junctional permeability [17]. Similarly, we saw a reduction of the P2 and P1 bands of Cx43 in astrocytes after siRNA-mediated Drebrin depletion (Figure 4C, lower panel). Therefore, it is tempting to speculate that Drebrin in astrocytes (most likely in complex with other submembrane proteins) may favor the functional stabilization of Cx43 at the plasma membrane. A reduction in the cellular level of Drebrin will destabilize Cx43 and may (directly or indirectly) influence other connexins that are expressed in astrocytes. Depletion of Drebrin facilitates the removal of connexins from the plasma membrane (as we observed for Cx43-GFP after siRNA-mediated Drebrin depletion in Vero cells; Figure 4B, right panel) and thus decreases cell-cell coupling.

Drebrin May Serve as a Linker between Cx43 and the Submembrane Cytoskeleton

In this paper we have demonstrated that Drebrin, which we found by a proteomics screen in a brain homogenate

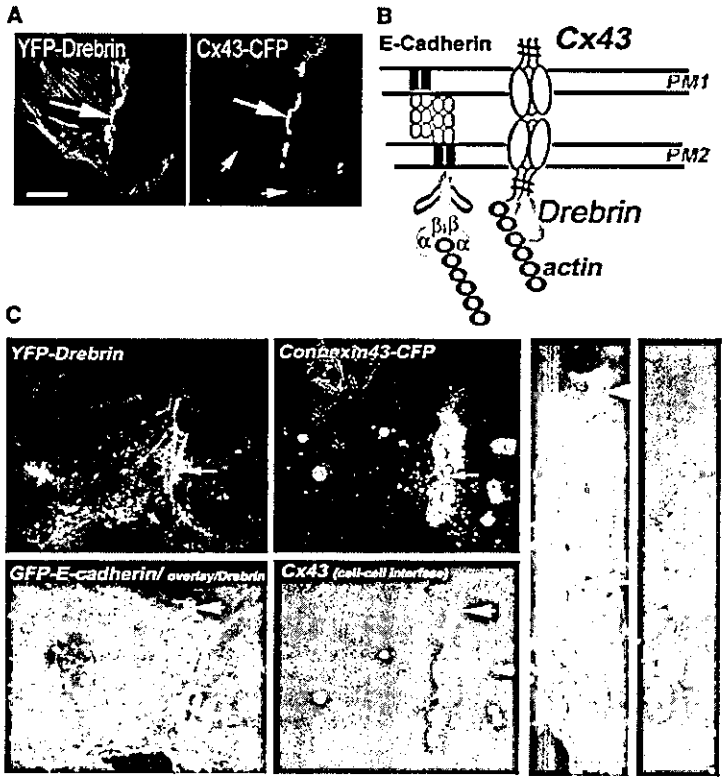

Figure 5. Intracellular Function of the Drebrin/Cx43 Interaction

(A) In Vero cells cotransfected with CFP-Drebrin and Cx43-YFP, both proteins are colocalized under the plasma membrane in the region of cell-cell contacts (big arrows) but not underneath the noncontacting plasma membrane regions (small arrows).

(B) Model introducing a comparison between the E-Cadherin/β-catenin/α-catenin/actin system and the novel Cx43/Drebrin/actin interactions discussed here.

(C) Plasma membrane interface of two cells cotransfected with Cx43-CFP, GFP E-cadherin, and CFP-Drebrin. Cx43-CFP is located mainly in the middle of the cell-cell interface, whereas GFP-E-cadherin is present mainly at the distal parts of the cell-cell interface. Drebrin is preferentially localized in the region labeled by Cx43-CFP and less in the distal parts labeled by GFP-E-cadherin.

fraction, not only colocalizes with Cx43 underneath the plasma membrane but also interacts with the C-terminal domain of Cx43 in a living cell, as analyzed by FRET (Figure 2). Drebrin and Cx43 cotransfected into Vero cells with fluorescent tags (CFP and YFP, respectively) were both present in zones of cell-cell contact (Figures 2A–2C and 5A). Initially, Drebrin had been described as an actin binding protein [18]. Additionally, a scaffolding role of Drebrin in the submembrane cytoskeleton of dendritic spines has been documented [19, 20]. Precedents for the regulation and stabilization of cell-cell contacts via crucial interactions with cytoplasmic proteins, (e.g., cell-cell adhesion mediated by E-cadherin) are well described [21]. In light of this, we consider it likely that Drebrin functions as a linker between gap junctions and the actin/submembrane cytoskeleton. We hypothesize that there is an analogy between the E-cadherin/β-catenin/α-catenin/actin system [21, 22] and the Cx43/Drebrin/actin system (as depicted in Figure 5B). Cx43 as well as E-cadherin may be utilized not only for cell–cell contacts but also to convey extracellular signals to their intracellular effectors by using Drebrin for the modification of the submembrane cytoskeleton in response to extracellular stimuli. This function may be fulfilled by Cx43 hemichannels that exist in the noncontacting membranes. As a first step to address this, we compared the intracellular distribution of E-cadherin, Cx43, and Drebrin. We cotransfected Vero cells with GFP-E-cadherin, Cx43-CFP, and YFP-Drebrin and linearly separated the fluorescent signals. The distribution of GFP-E-cadherin and Cx43-YFP in transfected Vero cells revealed that the initial interface between two cells was defined by E-cadherin pointed cell-cell contacts, whereas Cx43 was not present at the initial points of cell-cell contact (data not shown here). After a stable cell-cell contact interface was established by E-cadherin, Cx43-CFP started to accumulate in the middle region of this cell-cell interface (Figure 5C). Finally, in established cell-cell contacts Drebrin colocalizes more with Cx43 than with E-cadherin, suggesting that the Cx43/Drebrin complex may laterally displace E-cadherin together with cadherin-interacting proteins to the distal parts of this cell-cell interface. One of the previously described interacting partners of Cx43 underneath the plasma membrane is ZO-1 [5, 6]. ZO-1 has also been reported to bind cadherin molecules that appear to regulate the translocation of ZO-1 to the cell surface through interaction with catenins [23, 24]. In cases where Cx43 and E-cadherin are segregated during the formation of cell-cell contact interfaces, the relative strength of these interactions will determine the cellular distribution of ZO-1.

Intriguingly, Drebrin levels have been shown decrease during Alzheimer's disease (AD) [10, 25]. Thus, our single-cell experiments with siRNA-mediated depletion of Drebrin may somehow mimic the decreased level of Drebrin in AD, causing increased degradation of Cx43 and consequently impairing cell-cell coupling. Interestingly, Cx43 immunoreactivity was elevated at sites of amyloid plaques of Alzheimer's patients [26]. Our data allow us to speculate that the increased Cx43 expression in AD may represent an attempt of tissues to main-

tain homeostasis by aberrant induction of Cx43 expression in the pathological microenvironment of amyloid plaques. A similar mechanism of induction has been recently described for β-catenin, whose level is boosted by the loss of the noncanonical Wnt pathway [27].

In this study, we provide evidence for Drebrin as a novel and important interacting partner of Cx43 at the plasma membrane and show that it stabilizes Cx43-containing gap junctions in their functional state. Once gap junction plaques were formed, CFP-Drebrin still colocalized with Cx43-YFP in Vero cells even after Latrunculin B treatment, suggesting that the presence of actin filaments is not crucial for the Drebrin/Cx43 interaction. Interestingly, in mature hippocampal neurons the PSD-95 clusters containing Drebrin are also insensitive to Latrunculin A, suggesting that PSD-95 distribution is independent of the actin cytoskeleton [31]. In contrast, in developing neurons the synaptic clustering is still sensitive to Latrunculin A [20].

Depletion of Drebrin causes Cx43 to be targeted to a degradative pathway. Potentially, the cytoplasmic C-terminal domain of Cx43 is a highly regulated region that contains multiple motifs for protein-protein interactions. Interaction partners will likely include different kinases and molecules that recognize the Cx43 COOH terminus in its phosphorylated state, molecules containing PDZ, SH2, and SH3 domains, and components of the cellular ubiquitination machinery. In a very simple model, during gap junction formation Drebrin may bind to the C-terminal domain of Cx43 and thus sterically prevent interactions with other modifying molecules. Alternatively, Drebrin may stabilize Cx43 in its functional state as part of a larger submembrane cytoskeleton complex.

Experimental Procedures

GST-COOH-Terminus-Cx43 Construct; GFP Constructs

To create the GST-COOH-Cx43 (amino acids 234–382) construct, the relevant part of rat Cx43 [28] amplified by PCR. The sequences of the primers were as follows: forward primer, 5′-CTAGGGATC CAAGGGCGTTAAGGATCGCGTGAAG-3′; and reverse primer, 5′-CTA GGCGGCCGCTTAAATCTCCAGGTCATCAGG-3′. The PCR product was restricted with Bam HI and Not I and ligated into the Bam HI/Not I sites of pGEX-4T-3 (Pharmacia). A cDNA encoding human Drebrin E (accession number D17530; [29]) was used for generation of the CFP-Drebrin construct. Cloning of PCR fragments was used for generation of the YFP-, CFP- and GFP-tagged versions of full-length rat Cx43 used in this study. All constructs were verified by DNA sequencing.

Expression and Purification of GST-COOH-Cx43 Protein; GST Pull-Down Assay

GST-COOH-Cx43 protein was expressed in *E. coli* XL1 blue cells at 24°C in the presence of 100 μM IPTG and purified on Glutathione Sepharose 4B beads.

A fresh mouse brain was homogenized with 2 ml of internal medium containing "Complete" protease inhibitor (Roche). The homogenate was centrifuged 45 min at 100,000 g_{av} at 4°C. The supernatant was used in experiments as the "cytosol fraction." The pellet was resuspended in 2 ml of the same buffer, containing Triton X-100 to 1%, and centrifuged as described. The supernatant was used in experiments as the "membrane fraction."

The brain fractions were precleared by incubation with 50 μg of GST for 2 hr at 4°C on a rotating platform. A 20% suspension of glutathione sepharose 4B beads (300 μl) was added after the first 1 hr of this incubation. The samples were centrifuged at 500 g for 3 min, and the supernatant was used. The precleared fractions were then incubated with 300 μl of Glutathione Sepharose 4B beads loaded with GST fusion protein for 1.5 hr at 4°C on a rotating platform. Beads were washed five times in internal medium, containing "Complete" protease inhibitors (Roche) and 1% Triton X-100. The samples were boiled for 2 min in 60 μl 2× SDS-PAGE sample buffer containing 0.1% β-mercaptoethanol. The liquid phases were collected, and proteins were separated on 12% SDS-PAGE gels.

siRNA

siRNA duplexes against human Drebrin E (also called Drebrin I) (5′-CCAGAAGGUGAUGUACGGCdTdT-3′ sense and 3′-dTdTGGUCU UCCACUACAUGCCG-5′antisense) "Option C," nonlabeled or labeled with Cy3 on the 5′ end of the sense strand, were produced by Dharmacon (http://www.Dharmacon.com/).

Cell Culture and Transfection

Vero (ATCC) as well primary cultures of astrocytes obtained from mice brain were used in experiments. Cells were maintained in Dulbecco's modified Eagles medium, supplemented with 10% fetal calf serum, penicillin/streptomycin (100 μg/ml), and L-glutamine (2 mM). Transfection of Vero cells was performed by electroporation [11]. Transiently transfected cells (6–16 hr) were used in experiments. Oligofectamine reagent (Invitrogen) was used for siRNA transfection according to the manufacturers' instructions. For cotransfection with siRNA and DNA, cells were electroporated as described earlier except that the buffer was prepared with deionized RNAase-free water. siRNA-transfection with Oligofectamine was followed 24 hr thereafter by transfection with Cx43-GFP or GFP-actin-encoding plasmids. Expression patterns were analyzed within 6–18 hr after transfection with plasmids.

Immunocytochemistry

To study the cellular distribution of endogenous Cx43 and Drebrin, we fixed Vero cells and astrocytes in 3% PFA in the presence of FCS, washed the cells, and then permeabilized them with 0.1% saponin/3% BSA in PBS. Commercial antibodies against Cx43 (Sigma C6219) and a monoclonal antibody M2F6 against Drebrin (Stressgen) were used in combination with Cy3- and Cy2-labeled secondary antibodies. Cells were mounted in Fluorosave (Calbiochem) and analyzed with a Zeiss Axiovert 100 microscope.

FRET Analyses

CFP-Drebrin (donor) and Cx43-YFP (acceptor) were coexpressed in Vero cells for 6–12 hr. FRET (acceptor bleach) was applied for analysis of donor-acceptor interactions as described previously [11, 12]. In brief, Dbb (donor before bleach) and Abb (acceptor before bleach) images were acquired with a Zeiss Axiovert 100 TV fluorescence microscope equipped with 100× 1.4 NA Plan Apochromate objective lens, a CCD camera (Kodak, Princeton Instruments), and CFP and YFP filter sets (Omega Optics and AF Analytic, Germany). An increase in donor fluorescence was monitored with an excitation filter set that consisted of the following: for excitation, BP 430/20; and for emission, BP 485/17. Images were analyzed with MetaMorph 6.0 (Universal Imaging Corporation, West Chester, PA). After acquisition of Dbb and Abb images, the acceptor was photoinactivated with a green laser λ_{ex} 530 nm built into the Zeiss Axiovert 100, and two other images, Dab (donor after bleach) and Aab (acceptor after bleach), were recorded.

Supplemental Data

Supplemental Data including additional Experimental Procedures (surface biotinylation and subcellular fractionation; immunoprecipitation; immunoelectron microscopy [30]) and a table (peptide summary report) are available with this article online at http://www.current-biology.com/cgi/content/full/14/8/650/DC1/.

Acknowledgments

We are grateful to K. Lilley (Cambridge Centre for Proteomics) for MALDI Q-TOF analysis used for protein identification. We thank H.-D. Söling for his support and helpful discussions, S. Elbashir and J. Harborth for assistance with the siRNA experiments, and K. Weber for helpful comments (all at the Max-Planck Institute for Biophysical

Chemistry, Göttingen, Germany). We thank G. Söhl, K.Willecke, and M. Falk for Cx43 plasmids, J. Nelson and R. Kemler for GFP-E-cadherin plasmids, S. Kuznetsov for the GFP-actin plasmid, comments, and support, and M. Dale (Cambridge, UK) for expert technical assistance. We also thank D. Goodenough for reading an early version of this manuscript and suggesting useful experiments and M.S. Robinson for critical reading of an advanced text version. This work was supported by the Wellcome Trust (Senior Fellowship to R.D.; grant number 047578), the Deutsche Forschungsgemeinschaft (DFG grant So 43/60-1), and a Sonderforschungsbereich 406 grant to S.H.

Received: December 8, 2003
Revised: February 26, 2004
Accepted: March 10, 2004
Published: April 20, 2004

References

1. Kumar, N.M., and Gilula, N.B. (1996). The gap junction communication channel. Cell *84*, 381–388.
2. Goldberg, G.S., Lampe, P.D., and Nicholson, B.J. (1999). Selective transfer of endogenous metabolites through gap junctions composed of different connexins. Nat. Cell Biol. *1*, 457–459.
3. Bukauskas, F.F., Jordan, K., Bukauskiene, A., Bennett, M.V., Lampe, P.D., Laird, D.W., and Verselis, V.K. (2000). Clustering of connexin 43-enhanced green fluorescent protein gap junction channels and functional coupling in living cells. Proc. Natl. Acad. Sci. USA *97*, 2556–2561.
4. Willecke, K., Eiberger, J., Degen, J., Eckardt, D., Romualdi, A., Guldenagel, M., Deutsch, U., and Sohl, G. (2002). Structural and functional diversity of connexin genes in the mouse and human genome. Biol. Chem. *383*, 725–737.
5. Toyofuku, T., Yabuki, M., Otsu, K., Kuzuya, T., Hori, M., and Tada, M. (1998). Direct association of the gap junction protein connexin-43 with ZO-1 in cardiac myocytes. J. Biol. Chem. *273*, 12725–12731.
6. Giepmans, B.N., and Moolenaar, W.H. (1998). The gap junction protein connexin-43 interacts with the second PDZ domain of the zona occludens-1 protein. Curr. Biol. *8*, 931–934.
7. Giepmans, B.N., Verlaan, I., Hengeveld, T., Janssen, H., Calafat, J., Falk, M.M., and Moolenaar, W.H. (2001). Gap junction protein connexin-43 interacts directly with microtubules. Curr. Biol. *11*, 1364–1368.
8. Giepmans, B.N., Hengeveld, T., Postma, F.R., and Moolenaar, W.H. (2001). Interaction of c-Src with gap junction protein connexin-43. Role in the regulation of cell-cell communication. J. Biol. Chem. *276*, 8544–8549.
9. Asada, H., Uyemura, K., and Shirao, T. (1994). Actin-binding protein, drebrin, accumulates in submembranous regions in parallel with neuronal differentiation. J. Neurosci. Res. *38*, 149–159.
10. Shim, K.S., and Lubec, G. (2002). Drebrin, a dendritic spine protein, is manifold decreased in brains of patients with Alzheimer's disease and Down syndrome. Neurosci. Lett. *324*, 209–212.
11. Majoul, I.V., Bastiaens, P.I., and Soling, H.D. (1996). Transport of an external Lys-Asp-Glu-Leu (KDEL) protein from the plasma membrane to the endoplasmic reticulum: studies with cholera toxin in Vero cells. J. Cell Biol. *133*, 777–789.
12. Majoul, I., Straub, M., Hell, S.W., Duden, R., and Soling, H.D. (2001). KDEL-cargo regulates interactions between proteins involved in COPI vesicle traffic: measurements in living cells using FRET. Dev. Cell *1*, 139–153.
13. Majoul, I., Straub, M., Duden, R., Hell, S.W., and Soling, H.D. (2002). Fluorescence resonance energy transfer analysis of protein-protein interactions in single living cells by multifocal multiphoton microscopy. J. Biotechnol. *82*, 267–277.
14. Elbashir, S.M., Harborth, J., Weber, K., and Tuschl, T. (2002). Analysis of gene function in somatic mammalian cells using small interfering RNAs. Methods *26*, 199–213.
15. Lin, R., Warn-Cramer, B.J., Kurata, W.E., and Lau, A.F. (2001). v-Src phosphorylation of connexin 43 on Tyr247 and Tyr265 disrupts gap junctional communication. J. Cell Biol. *154*, 815–827.
16. TenBroek, E.M., Lampe, P.D., Solan, J.L., Reynhout, J.K., and Johnson, R.G. (2001). Ser364 of connexin43 and the upregulation of gap junction assembly by cAMP. J. Cell Biol. *155*, 1307–1318.
17. Faucheux, N., Zahm, J.M., Bonnet, N., Legeay, G., and Nagel, M.D. (2004). Gap junction communication between cells aggregated on a cellulose-coated polystyrene: influence of connexin 43 phosphorylation. Biomaterials *25*, 2501–2506.
18. Ishikawa, R., Hayashi, K., Shirao, T., Xue, Y., Takagi, T., Sasaki, Y., and Kohama, K. (1994). Drebrin, a development-associated brain protein from rat embryo, causes the dissociation of tropomyosin from actin filaments. J. Biol. Chem. *269*, 29928–29933.
19. Shirao, T., and Sekino, Y. (2001). Clustering and anchoring mechanisms of molecular constituents of postsynaptic scaffolds in dendritic spines. Neurosci. Res. *40*, 1–7.
20. Takahashi, H., Sekino, Y., Tanaka, S., Mizui, T., Kishi, S., and Shirao, T. (2003). Drebrin-dependent actin clustering in dendritic filopodia governs synaptic targeting of postsynaptic density-95 and dendritic spine morphogenesis. J. Neurosci. *23*, 6586–6595.
21. Jamora, C., and Fuchs, E. (2002). Intercellular adhesion, signalling and the cytoskeleton. Nat. Cell Biol. *4*, E101–E108.
22. Yonemura, S., Itoh, M., Nagafuchi, A., and Tsukita, S. (1995). Cell-to-cell adherens junction formation and actin filament organization: similarities and differences between non-polarized fibroblasts and polarized epithelial cells. J. Cell Sci. *108*, 127–142.
23. Itoh, M., Nagafuchi, A., Moroi, S., and Tsukita, S. (1997). Involvement of ZO-1 in cadherin-based cell adhesion through its direct binding to alpha catenin and actin filaments. J. Cell Biol. *138*, 181–192.
24. Rajasekaran, A.K., Hojo, M., Huima, T., and Rodriguez Boulan, E. (1996). Catenins and zonula occludens-1 form a complex during early stages in the assembly of tight junctions. J. Cell Biol. *132*, 451–463.
25. Harigaya, Y., Shoji, M., Shirao, T., and Hirai, S. (1996). Disappearance of actin-binding protein, drebrin, from hippocampal synapses in Alzheimer's disease. J. Neurosci. Res. *43*, 87–92.
26. Nagy, J.I., Li, W., Hertzberg, E.L., and Marotta, C.A. (1996). Elevated connexin-43 immunoreactivity at sites of amyloid plaques in Alzheimer's disease. Brain Res. *717*, 173–178.
27. Westfall, T.A., Hjertos, B., Twedt, J., Brimeyer, R., Gladon, J., Olberding, A., Furutani-Seiki, M., and Slusarski, D.C. (2003). Wnt-5/pipetail functions in vertebrate axis formation as a negative regulator of Wnt/β-catenin activity. J. Cell Biol. *162*, 889–898.
28. Falk, M.M., Kumar, N.M., and Gilula, N.B. (1994). Membrane insertion of gap junction connexins: polytopic channel forming membrane proteins. J. Cell Biol. *127*, 343–354.
29. Toda, M., Shirao, T., Minoshima, S., Shimizu, N., Toya, S., and Uyemura, K. (1993). Molecular cloning of cDNA encoding human drebrin E and chromosomal mapping of its gene. Biochem. Biophys. Res. Commun. *196*, 468–472.
30. Tokuyasu, K.T. (1978). A study of positive staining of ultrathin frozen sections. J. Ultrastruct. Res. *63*, 287–307.
31. Allison, D.W., Chervin, A.S., Gelfand, V.I., and Craig, A.M. (2000). Postsynaptic scaffolds of excitatory and inhibitory synapses in hippocampal neurons: maintenance of core components independent of actin filaments and microtubules. J. Neurosci. *20*, 4545–4554.

HIPPOCAMPUS 13:845–858 (2003)

Increased Levels of Acidic Calponin During Dendritic Spine Plasticity After Pilocarpine-Induced Seizures

Lotfi Ferhat,[1*] Monique Esclapez,[1] Alfonso Represa,[1]
Abdellatif Fattoum,[2] Tomoaki Shirao,[3]
and Yezekiel Ben-Ari[1]

[1]*INMED/INSERM U29, Marseille Cedex, France*
[2]*CRBM-UPR 1086, Montpellier Cedex, France*
[3]*Department of Neurology and Behavior,*
Gunma University School of Medicine, Maebashi, Gunma, Japan

ABSTRACT: **We have previously shown that, in HEK 293 cells, overexpression of acidic calponin, an actin-binding protein, induces remodeling of actin filaments, leading to a change in cell morphology. In addition, this protein is found in dendritic spines of adult hippocampal neurons. We hypothesized that this protein plays a role in regulating actin-based filaments during dendritic spine plasticity. To assess this hypothesis, the pilocarpine model of temporal lobe epilepsy was selected because an important reorganization of the glutamatergic network, which includes an aberrant sprouting of granule cell axons, neo-synaptogenesis, and dendritic spine remodeling, is well established in the dentate gyrus. This reorganization begins after the initial period of status epilepticus after pilocarpine injection, during the silent period when animals display a normal behavior, and reaches a plateau at the chronic stage when the animals have developed spontaneous recurrent seizures. Our data show that the intensity of immunolabeling for acidic calponin was clearly increased in the inner one-third of the molecular layer of the dentate gyrus, the site of mossy fiber sprouting, and neo-synaptogenesis, at 1 and 2 weeks after pilocarpine injection (silent period) when the reorganization was taking place. In contrast, in chronic pilocarpine-treated animals, when the reorganization was established, the levels of labeling for acidic calponin in the inner molecular layer were similar to those observed in control rats. In addition, double immunostaining studies suggested that the increase in acidic calponin levels occurred within the dendritic spines. Altogether, these results are consistent with an involvement of acidic calponin in dendritic spine plasticity.** © 2003 Wiley-Liss, Inc.

KEY WORDS: **epilepsy; actin; spine formation; drebrin; rat**

INTRODUCTION

Dendritic spines are the main target on which the majority of excitatory glutamatergic synapses have been found in the central nervous system (Gray, 1959; Peters et al., 1976; Parnavelas et al., 1977) and may function as units of synaptic integration (Harris and Kater, 1994; Yuste and Tank, 1996). The shape and density of dendritic spines appear to be influenced by several factors, including age, hormones, neurotrophins, disease, learning, and synaptic activity (Bailey and Kandel, 1993; Horner, 1993; Harris and Kater, 1994). In addition, this plasticity of the spines may be involved in long-term memory storage (Crick, 1982; Bailey and Kandel, 1993). Indeed, long-term potentiation (LTP), a persistent enhancement of synaptic strength that is believed to underlie learning and memory, has been associated with both altered spine morphology (Desmond and Levy, 1988; Fifkova and Morales, 1992; Hosokawa et al., 1995; Toni et al., 1999; Lee and Sheng, 2000) and emergence of new spines (Engert and Bonhoeffer, 1999; Maletic-Savatic et al., 1999).

Dendritic spines are highly enriched with actin filaments (Fifkova and Delay, 1982; Matus et al., 1982), which are thought to be involved in spine plasticity (Smith, 1999; Van Rossum and Hanisch, 1999; Matus, 2000; Rao and Craig, 2000). The identification of the molecular basis responsible for spine plasticity is fundamental in order to understand the mechanisms of synaptic plasticity.

We hypothesized that acidic calponin, an actin-binding protein, is one of the regulators of actin filaments during spine plasticity based on the following observations: (1) electron microscopic studies have shown that this protein is within dendritic spines in adult hippocampal neurons (Agassandian et al., 2000); (2) transfection of acidic calponin into HEK 293 cells induced remodeling of actin filaments, which led to changes in cell morphol-

Abbreviations used: DG, dentate gyrus; G, granule cell layer; GFAP, glial fibrillary acidic protein; H, hilus; IgG, immunoglobulin G; IHC, immunohistochemistry; IML, inner molecular layer; KPBS, potassium phosphate-buffered saline; LTP, long-term potentiation; M, molecular layer; MAP2, microtubule-associated protein; PB, phosphate-buffer; RT, room temperature.

Grant sponsor: Institut National de la Santé et de la Recherche Médicale (INSERM).

*Correspondence to: Lotfi Ferhat, INMED/INSERM U29, 163 rue de Luminy, BP 13, 13273, Marseille Cedex 09, France.
E-mail: ferhat@inmed.univ-mrs.fr

Accepted for publication 10 December 2002
DOI 10.1002/hipo.10136

ogy (Ferhat et al., 2001); and (3) the calponin family stimulates actin polymerization, bundling and stabilization of F-actin filaments (Kake et al., 1995; Kolakowski et al., 1995; Danninger and Gimona, 2000; Ferhat et al., 2001).

In the present study, we tested our hypothesis, relying on a well-characterized experimental model of temporal lobe epilepsy induced by pilocarpine in adult rats. In this model, an important aberrant sprouting of granule cell axons (mossy fibers) (Mello et al., 1993; Okazaki et al., 1995) is reported. In normal conditions, mossy fibers innervate CA3 pyramidal neurons as well as hilar mossy cells and interneurons (Amaral et al., 1990; Ribak and Peterson, 1991; Wenzel et al., 1997; Acsady et al., 1998). After pilocarpine-induced seizures, mossy fibers sprout and form new functional synapses on the granule cell dendrites in the inner molecular layer (IML) of the dentate gyrus (DG) (Okazaki et al., 1995; Okazaki and Nadler, 2001; Buckmaster et al., 2002). Moreover, the sprouting of mossy fibers is associated with a remodeling of dendritic spine shape and density of dentate granule cells (Isokawa, 1998, 2000). Thus, if acidic calponin is involved in spine plasticity, we would expect an increase in this protein during the morphological reorganization observed in pilocarpine-induced seizures. Indeed, our data showed that the acidic calponin levels were strongly increased in the inner one-third of the molecular layer of the DG 1 or 2 weeks after pilocarpine-induced seizures. Furthermore, double immunohistochemical studies for acidic calponin and drebrin, an actin-binding protein specifically localized in dendritic spines, suggested that the increase in acidic calponin levels occurred within dendritic spines of presumed granule cells. These results are consistent with an involvement of acidic calponin in the plasticity of dendritic spines.

MATERIALS AND METHODS

Animals

Experiments involving animals were approved by the European Communities Council (86/609/EEC). Adult male Wistar rats weighing 200–290 g (Charles River, France) were injected intraperitoneally (i.p.) with pilocarpine hydrochloride (325–350 mg/kg; Sigma, St. Louis, MO), a muscarinic cholinergic agonist. The injection protocols were similar to those previously described (Turski et al., 1983; Cavalheiro et al., 1987; Obenaus et al., 1993). A low dose of the cholinergic antagonist methylscopolamine nitrate (1 mg/kg, i.p.) was administrated 30 min before pilocarpine injection, to reduce the agonist peripheral cholinergic effects (Baez et al., 1976; Turski et al., 1983). Only animals that displayed robust behavioral seizures for 3–4 h were selected in this study. This period of severe sustained seizures was stopped by a single injection of valium (6 mg/kg, i.p.; Sigma), to reduce mortality among these animals. The rats were then observed periodically in the vivarium for general behavior and occurrence of spontaneous seizures for a period of 16 weeks. Pilocarpine-treated animals were studied at several post-injection intervals: during the silent period, when animals displayed an apparent normal behavior (1 and 2 weeks, n = 4 at each interval) and during the chronic stage, when the animals had developed spontaneous recurrent limbic seizures (16 weeks, n = 4). The onset of spontaneous seizure occurrence was 4–6 weeks after pilocarpine injection. Eight age-matched rats from the same litters were used for control experiments.

Tissue Preparation

The rats were deeply anesthetized with sodium pentobarbital (60 mg/kg, i.p.) and perfused through the heart with a fixative solution (1 ml/g body weight) of 4% paraformaldehyde in 0.12 M phosphate buffer, pH 7.3 (PB). After perfusion, brains were removed from the skull, post-fixed in the same fixative for 1 h at room temperature (RT), rinsed in 0.12 M PB for 1.5 h, and immersed in a cryoprotective solution of 20% sucrose in PB overnight at 4°C. Blocks of brain which contained the entire hippocampal formation were quickly frozen on dry ice and sectioned coronally with a cryostat (40 μm thick). The sections obtained were rinsed in PB, collected sequentially into 1-ml microcentrifuge tubes containing an ethylene glycol-based cryoprotective solution (Watson et al., 1986; Lu and Haber, 1992), and stored at −20°C until used for immunohistochemistry (IHC).

Primary Antibodies

Antibodies were obtained from various sources. Acidic calponin was detected with a polyclonal antiserum raised in rabbits against the C-terminal of the rat protein. The specificity of this antiserum has been previously assessed by Western blot on the total homogenate of rat hippocampus (Plantier et al., 1999). Drebrin was localized with a mouse monoclonal antibody (M2F6; Shirao and Obata, 1986). The mouse monoclonal antibody against synaptophysin (Chemicon, Temecula, CA), mouse monoclonal antibody against microtubule-associated protein 2 (MAP2; Sigma), and mouse monoclonal antibody against glial fibrillary acidic protein (GFAP; Roche Diagnostics, Meylan, France) were purchased as indicated.

Immunohistochemistry

Single immunohistochemical labeling for acidic calponin, synaptophysin, and MAP2 was performed with standard avidin-biotin-peroxidase methods (Vectastain ABC kit; Vector Laboratories, Burlingame, CA). Free-floating sections were rinsed for 30 min in PB, incubated in 1% H_2O_2 (Sigma) for 40 min in PB to block endogenous peroxidase activity, and rinsed for 30 min in 0.02 M potassium phosphate-buffered saline (KPBS; 16 mM K_2HPO_4, 3.5 mM KH_2PO_4, 150 mM NaCl, pH 7.4). Sections processed for acidic calponin-IHC were preincubated for 1 h at RT in KPBS containing 0.3% Triton X-100 (Sigma) and 3% normal goat serum (Vector) and then incubated overnight at room temperature (RT) in the acidic calponin polyclonal antiserum (1:300) diluted in KPBS containing 0.3% Triton X-100 and 1% normal goat serum. Sections processed for synaptophysin- and MAP2-IHC were preincubated for 1 h at RT in KPBS containing 0.3% Triton X-100 and 3% normal horse serum (Vector) and then incubated overnight at RT in either synaptophysin (1:200) or

MAP2 (1:500) monoclonal antibodies diluted in KPBS containing 0.3%, Triton X-100 and 1% normal horse serum. The following day, sections were rinsed in KPBS, incubated for 1 h at RT in biotinylated goat anti-rabbit IgG (1:200; Vector) or horse anti-mouse IgG (1:200; Vector) in KPBS containing 3% normal goat serum or normal horse serum. Sections were then rinsed in KPBS, incubated for 1 h at RT in the avidin-biotin-peroxidase solution prepared in KPBS according to manufacturer's recommendations. After several rinses in KPBS, sections from control and pilocarpine-treated animals were processed for the same period of time in 0.05% 3-3'-diaminobenzidine-HCl (Sigma) and 0.006% H_2O_2 diluted in KPBS. The sections were then rinsed in KPBS, mounted on gelatin-coated slides, dried, dehydrated and coverslipped with Permount (Fischer Scientific, Electron Microscopy Sciences, Washington, PA).

Quantitative Analysis

Semiquantitative analyses of the intensity of immunolabeling for acidic calponin, synaptophysin, and MAP2 were conducted in the granule cell layer (G) and inner molecular layer (IML) of the dentate gyrus to identify differences between control and pilocarpine animals. This analysis of the labeling intensity was performed by optical densitometric measurements of the labeling with an image analyzing system according to previously described methods (Larsson et al., 1991; Larsson and Hougaard, 1993, 1994a,b; Esclapez and Houser, 1999). The image analysis system used in this study included a PC-compatible computer, a Nikon digital camera DXM 1200 connected to a Nikon E800 microscope (Nikon, Melville, NY), a Nikon ACT-1 frame grabber, and NIH Image 1.62 software. All images were acquired with a 40× lens, under the same conditions of light illumination, with the microscope light source stabilized, and at a final digitized size of 640 × 480 pixels. The densitometric analysis of labeling was performed using NIH software, which automatically determined the gray level value. For each control and pilocarpine animal, quantitative data were obtained from the hippocampus on both sides in four sections. The analysis of labeling intensity was performed from a total of 16 microscopic fields per region of interest (G and IML). For each of these microscopic fields, the total gray level value was automatically obtained. The gray level value of the corpus callosum was used as a reference value for background. The specific intensity of labeling corresponding to the corrected gray level value was calculated by subtracting the gray level value of the background from the total gray level value. For each region of interest the mean and corresponding standard error to the mean (SEM) intensity of labeling obtained from the total number of microscopic fields were calculated for each series of control and pilocarpine-treated animals.

Statistical analysis of differences in the mean intensity of labeling for acidic calponin, synaptophysin, and MAP2 between control and pilocarpine-treated animals at each interval (1, 2, and 16 weeks) and each region of interest was carried out with a mixed-model analysis of variance (ANOVA) and Student's *t*-test.

Immunofluorescence

For double-immunofluorescence labeling of acidic calponin/GFAP, acidic calponin/synaptophysin, acidic calponin/MAP2, and acidic calponin/drebrin, sections were rinsed for 30 min in KPBS and preincubated for 1 h at RT in KPBS containing 0.3% Triton X-100 and 1% blocking reagent (Roche diagnostics, Meylan, France). Sections were then incubated overnight at RT in a mixture of acidic calponin antiserum (1:300) and either GFAP (1:100), synaptophysin (1:100), MAP2 (1:500) or drebrin (hybridoma supernatant) monoclonal antibodies diluted in KPBS containing 0.3% Triton X-100 and 1% blocking reagent. After several rinses in KPBS, sections were incubated for 1 h at RT in biotinylated goat anti-rabbit IgG (1:200), rinsed in KPBS and incubated in a mixture of Alexa 488-conjugated goat anti-mouse IgG (1:200, Jackson Immunoresearch, West Grove, PA) and Cy3-conjugated streptavidin (1:200, Jackson Immunoresearch) diluted in KPBS. The sections were then mounted on gelatin-coated slides and were dried and coverslipped with Fluoromount G (Southern Biotechnology Associates, Birmingham, AL). The specimens were analyzed with an Olympus fluoview-500 laser scanning microscope. In all cases, no labeling was detected when specific antibodies were replaced with normal rabbit or mouse serum or when primary antibodies were omitted.

RESULTS

The expression of different proteins of interest was followed in the granule cell and inner molecular layers of the dentate gyrus (DG). In these regions, a major aberrant sprouting of granule cell axons has been observed in pilocarpine-treated animals (Mello et al., 1993; Okazaki et al., 1995). Differences in labeling intensity were observed consistently in sections from all control and pilocarpine-treated animals for acidic calponin, synaptophysin and MAP2 in the granule cell and inner molecular layer of the DG.

Immunolabeling for Acidic Calponin Is Increased in the Dentate Gyrus After Pilocarpine-Induced Seizures

In control animals (Fig.1A), the immunohistochemical labeling for acidic calponin was observed in all layers of the dentate gyrus, including the hilus, the granule cell, and molecular layers. In the dendritic layers (hilus and molecular layer), labeling was evenly distributed (Fig. 1A,B). In addition to this diffuse neuronal staining, many astrocytes and cells located along the infragranular border of the DG were labeled for acidic calponin (Fig. 1B).

In pilocarpine-treated animals at 1 week (Fig. 1C,D) and 2 weeks (Fig. 1E,F), the pattern of labeling for acidic calponin was clearly modified, as compared with control rats (Fig. 1A,B). In these pilocarpine-treated animals, the inner one-third of the molecular layer (IML) was strongly labeled for acidic calponin (Fig. 1C–F). This high level of labeling contrasted with the levels of staining observed in the outer two-thirds of the molecular layer.

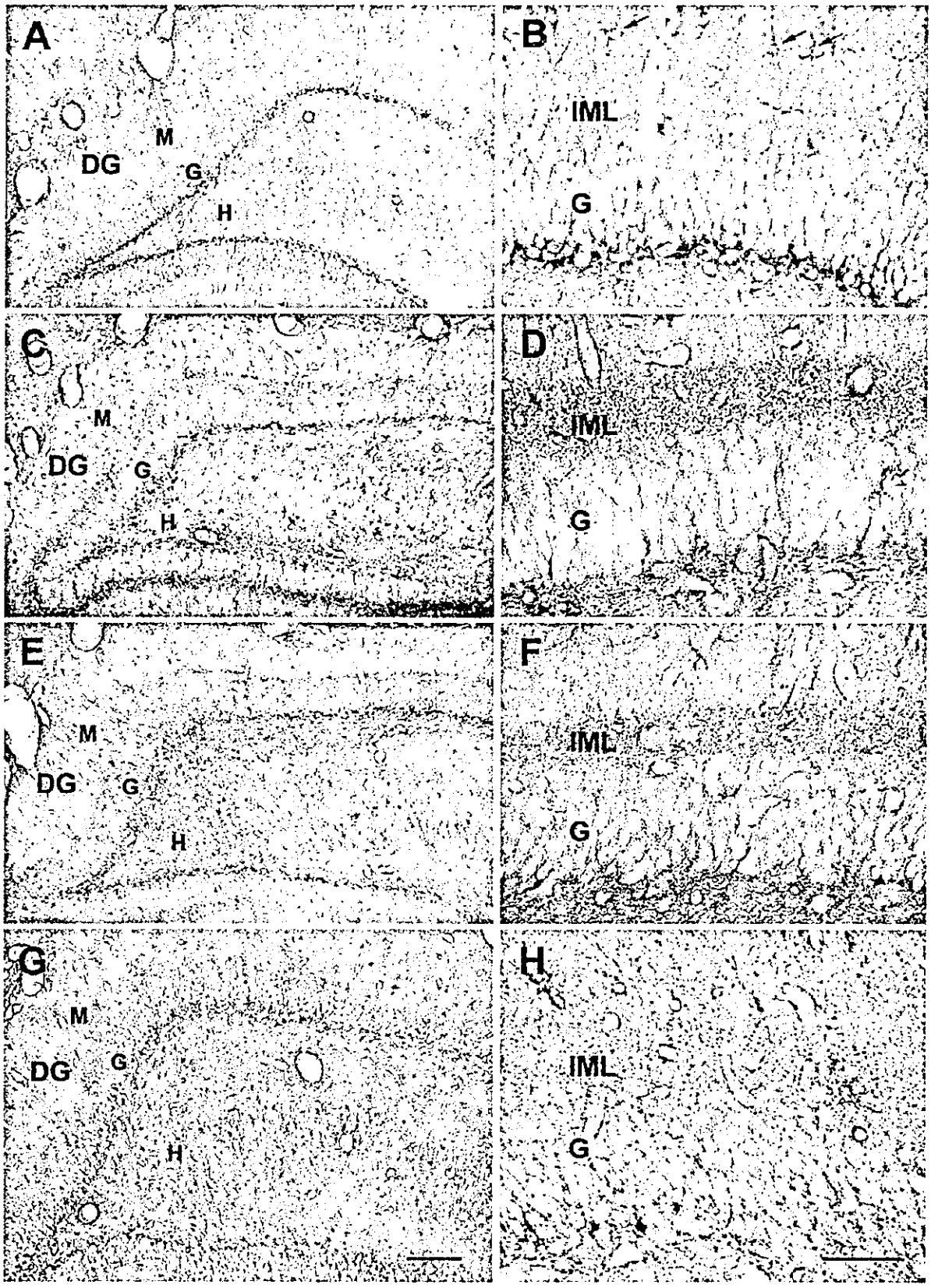

FIGURE 1.

Moderate to high increases in the labeling intensity for acidic calponin were also observed in the granule cell layer and in the hilus. The increases in these layers were mainly observed at 1 week, a time of strong reactive gliosis (Obenaus et al., 1993; see Fig. 5A,B). In contrast, in chronic pilocarpine-treated animals (16 weeks; Fig. 1G), the intensity of labeling for acidic calponin was strongly decreased in the IML of the DG, as compared with pilocarpine rats at 1 (Fig. 1C) and 2 weeks (Fig. 1E). Because in pilocarpine rats, the increased levels of labeling for acidic calponin occurred in the region of intense reorganization, including mossy fiber sprouting (Mello et al., 1993; Okazaki et al., 1995), outgrowth of granule cell dendrites (Parent et al., 1997) and dendritic spine plasticity (Isokawa, 1998, 2000), we further investigated whether acidic calponin expression was co-regulated with the expression of specific markers for both presynaptic (synaptophysin) and postsynaptic (MAP2) elements.

Immunolabeling Changes for Synaptophysin in the Dentate Gyrus After Pilocarpine-Induced Seizures

Immunolabeling for synaptophysin that labeled axon terminals has been reported previously in the hippocampal formation of adult rats (Masliah et al., 1991). We describe the staining obtained for synaptophysin in control rats to compare this labeling with that of pilocarpine-treated animals. Briefly, punctiform immunolabeling for synaptophysin was found in all layers of the dentate gyrus (Fig. 2). Within the molecular layer, synaptophysin immunoreactivity showed a trilaminar pattern with the inner and outer part displaying the strongest intensity of staining (Fig. 2A,B). A clear staining surrounding the cell bodies of granule cells was observed (Fig. 2B). The strong staining present in the hilus corresponds to the labeling of γ-aminobutyric acid (GABA)ergic and glutamatergic terminals including mossy fiber terminals (Fig. 3A).

The pattern of labeling for synaptophysin was different in pilocarpine-treated animals at all time intervals examined, as compared with that observed in control rats. One week after pilocarpine injection, the labeling intensity was clearly decreased in the inner one-third of the molecular layer (Fig. 2C,D). In contrast, the labeling intensity in all the other regions of the dentate gyrus including the hilus, the granular cell layer and the outer two-thirds of the molecular layer was relatively well preserved. The pattern of staining for synaptophysin was similar at 2 (Fig. 2E,F) and 16 weeks (Fig. 2G,H) after pilocarpine injection but differed from that found at 1 week (Fig. 2C,D) and in control animals (Fig. 2A,B). At 2 and 16 weeks, a strong intensity of labeling was present in the inner molecular layer. However, this high level of staining was restricted to the supragranular region of the inner molecular layer (Fig. 2F,H), in contrast to that observed in control animals (Fig. 2B). No major differences in labeling intensity were detected in the hilus, the granular cell layer and the outer molecular layer at 2 and 16 weeks (Fig. 2E–H) compared with control rats (Fig. 2A,B).

Immunolabeling for Microtubule-Associated Protein 2 Is Increased in the Dentate Gyrus After Pilocarpine-Induced Seizures

The pattern of immunohistochemical labeling for MAP2 in the hippocampal formation of control animals was similar to that previously described (Pollard et al., 1994). Briefly, MAP2 staining was present in all layers of the dentate gyrus including the hilus, granule cell and molecular layers (Fig. 3A,B). MAP2 labeling was evenly distributed in the molecular layer. The soma of granule cells was also clearly labeled for MAP2 (Fig. 3B) as many dendritic processes in the hilus (Fig. 3A). In pilocarpine-treated animals at 1 (Fig. 3C) and 2 weeks (Fig. 3E), a clear increase in MAP2 immunoreactivity was observed in the granular cell and molecular layers of the dentate gyrus (Fig. 3C–F). In addition to this general increase in the level of labeling, the pattern of staining for MAP2 clearly differed in the molecular layer of the dentate gyrus between pilocarpine-treated and control animals. This difference was due primarily to an increase in the labeling intensity, to a much greater extent in the inner one-third of the molecular layer than in the outer-two-thirds of this layer. In contrast, a decreased labeling for MAP2 was observed in the region beneath the granule cell layer as well as in the central part of the hilus including regions near the inner tip of CA3c and the apex (Fig. 3C,E), probably due to the loss of neurons described in this region (Obenaus et al., 1993). In chronic pilocarpine-treated animals (Fig. 3G), the intensity of labeling for MAP2 was strongly decreased in the inner one-third of the molecular layer (Fig. 3H), as compared with pilocarpine-treated rats at 1 (Fig. 3D) and 2 weeks (Fig. 3F).

Quantitative Analysis of the Changes in Acidic Calponin, Synaptophysin, and MAP2 Levels

Because differences in labeling intensity were observed consistently for acidic calponin, synaptophysin and MAP2 in the inner molecular layer of the dentate gyrus, we conducted semiquantative analysis in this layer and in the granule cell layer to determine the relative extent of these changes. Quantitative data showed that, in the inner molecular layer of the dentate gyrus, the mean intensities of labeling for acidic calponin were significantly increased in the pilocarpine animals at 1 (70%, 101.95 ± 1.05) and 2 weeks (48%, 88.63 ± 1.18), as compared with control rats (59.88 ± 1.43) (Fig. 4A, Table 1), whereas no difference was found in pilocarpine-treated animals at 16 weeks (59.14 ± 0.84) (Fig. 4A, Table 1). In the granule cell layer, the intensity of labeling was significantly increased in pilocarpine-treated animals at all time intervals examined (23%, 57.12 ± 0.89 at 1 week, 10%, 50.99 ± 0.86 at 2 weeks

FIGURE 1. Acidic calponin immunoreactivity in coronal sections of dentate gyrus from control and pilocarpine-treated animals. A,B: In a control rat, immunoreactivity of acidic calponin in the dentate gyrus (DG) is mainly present in astrocytes (arrows) and cells located along the infragranular region of the granule cell layer (G). A diffuse staining is evenly observed in all parts of the molecular layer (M) including the inner molecular layer (IML). C–H: Immunoreactivity of acidic calponin in the dentate gyrus of pilocarpine-treated rats at 1 week (C,D), 2 weeks (E,F), and 16 weeks (G,H). In pilocarpine-treated animals at 1 and 2 weeks, acidic calponin immunoreactivity was substantially increased in IML of the DG compared with control (A,B) and to pilocarpine-treated rats at 16 weeks (G,H). Scale bars = 200 μm in A,C,E,G; 50 μm in B,D,F,H.

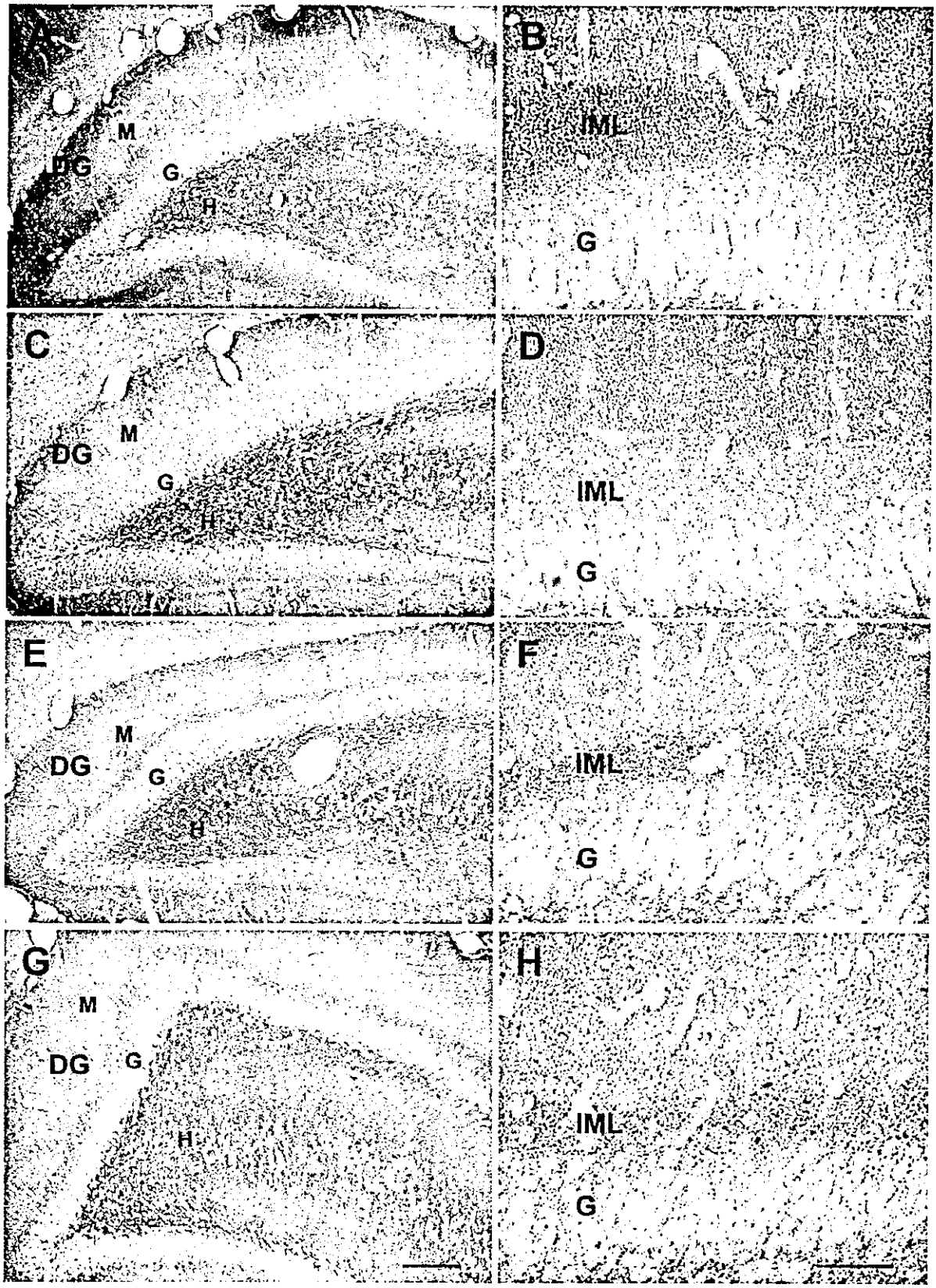

FIGURE 2.

and 12%, 52.23 ± 0.58 at 16 weeks), as compared with control (46.53 ± 1.14), but to a much lower extent than in the inner molecular layer. The intensities of labeling for synaptophysin in the inner molecular layer were significantly decreased in the pilocarpine-treated rats at 1 week (26%, 81.24 ± 2.33), and to a much lower extent at 2 (10%, 92.5 ± 2.87) and 16 weeks (7%, 95.28 ± 2.05), as compared with control (102.6 ± 1.94) (Fig. 4B, Table 1). In addition, the intensities of labeling in this layer were significantly increased at 2 (14%, $P < 0.01$) and 16 (17%, $P < 0.001$) weeks compared with 1 week. No difference in the mean intensity of labeling was found in the granule cell layer of pilocarpine-treated animals at any time interval (1 week 44.87 ± 1.03; 2 weeks 45.97 ± 1.41; 16 weeks 46.45 ± 1.05), as compared with control rats (47.43 ± 1.09) (Fig. 4B, Table 1). The mean intensity of labeling for MAP2 was significantly increased in pilocarpine-treated animals at all time intervals studied, in the inner molecular layer (24%, 103.1 ± 2.17 at 1 week; 22%, 105.33 ± 1.74 at 2 weeks; 6%, 84.15 ± 1.38 at 16 weeks) as well as in the granule cell layer (33%, 50.58 ± 1.18 at 1 week; 15%, 64.02 ± 1.57 at 2 weeks; 15%, 50.66 ± 1.64 at 16 weeks), as compared with control (IML: 80.01 ± 1.18; G: 43.06 ± 1.07) (Fig. 4C, Table 1). Thus qualitative, like quantitative, analyses showed that the changes in the pattern of labeling for acidic calponin in the molecular layer of the dentate gyrus in pilocarpine-treated animals paralleled those found for MAP2, known as a dendritic marker, at all time intervals examined in this study.

Immunolabeling for Acidic Calponin Was Absent From Presynaptic Sites But Was Localized in Dendritic Spines

Since acidic calponin is also expressed in glial cells (Ferhat et al., 1996; Plantier et al., 1999; present findings), we first investigated whether the increased labeling intensity for acidic calponin observed in the inner one-third of the molecular layer in pilocarpine-treated animals occurred in glial processes. For this purpose, double labeling for acidic calponin (red) and GFAP (green) was performed in pilocarpine-treated rats at 1 and 2 weeks. In these animals, several glial cells and their processes immunoreactive for GFAP were also labeled for acidic calponin (Fig. 5A,B). However, in all sections examined, most of the punctiform labeling for acidic calponin in the inner one-third of the molecular layer was not immunoreactive for GFAP (Fig. 5B), suggesting that the increased staining of acidic calponin occurred in neuronal compartments.

Because the punctiform staining of acidic calponin was located in the inner molecular layer, the region of mossy fiber sprouting, we wanted to determine whether this staining revealed presynaptic compartments. Thus, we completed double immunostaining for acidic calponin and synaptophysin, a specific marker for the presynaptic compartment. As illustrated in Figure 5C, both acidic calponin (red) and synaptophysin (green) displayed punctiform patterns. However, these two stains did not co-localize; instead, the two proteins were present in adjacent cellular compartments (Fig. 5C, inset), suggesting a postsynaptic localization of acidic calponin.

To identify the postsynaptic compartment, we performed double labeling for acidic calponin and specific markers for dendritic shafts (MAP2) or for spines (drebrin). Double staining with acidic calponin (red) and MAP2 (green) showed that these proteins were not co-localized (Fig. 5D), as spots labeled for acidic calponin appeared to be attached to dendritic shafts (Fig. 5D, inset). Double labeling for acidic calponin (red) and drebrin (green) showed that in control rats dendritic spines labeled for drebrin in the molecular layer of DG did not contain detectable levels of acidic calponin whereas in pilocarpine-treated rats at 1 and 2 weeks, some spines clearly contained acidic calponin in the inner molecular layer. Indeed, in control animals, many cellular elements were labeled either for acidic calponin or for drebrin in the granule cell and molecular layers of the DG (Fig. 6A,B). The two proteins were never co-localized in the same compartment (Fig. 6B). In pilocarpine-treated animals, many spines labeled only for drebrin and many cellular elements labeled only for acidic calponin (presumed glial processes) were present in the granule cell and molecular layers of the DG (Fig. 6C,D) as in control animals (cf. Fig. 6A,B with C,D). However, in contrast to control animals, some spines labeled for drebrin (Fig. 6C–E) were also labeled for acidic calponin in the pilocarpine-treated animals (Fig. 6C,D,F). These spines double-labeled for the two proteins were observed in the inner molecular layer of the DG (Fig. 6C). No co-localization was observed in the outer two-thirds of the molecular layer. These results indicated that, in pilocarpine-treated animals, acidic calponin protein was present in some dendritic spines of presumed granule cells.

FIGURE 2. Synaptophysin immunoreactivity in coronal sections of dentate gyrus from control and pilocarpine-treated animals. A,B: In a control rat, immunoreactivity of synaptophysin in the dentate gyrus (DG) is observed in the granule cell layer (G) and all dendritic layers including the hilus (H) and the molecular layer (M). In the latter layer, the staining was stronger in the inner and outer molecular layers than in the middle molecular layer. C–H: Immunoreactivity of synaptophysin in the dentate gyrus of pilocarpine-treated rats at 1 week (C,D), 2 weeks (E,F), and 16 weeks (G,H). In a pilocarpine-treated rat at 1 week, synaptophysin immunoreactivity was decreased in the inner one-third of the molecular layer (IML) of the DG, as compared with a control rat (cf. A with C and B with D). In pilocarpine-treated rats at 2 weeks and 16 weeks, synaptophysin immunoreactivity was increased in the inner one-third of the molecular layer (IML) of the DG, as compared with pilocarpine-treated animals at 1 week (cf. E and G with C and F and H with D). In control and pilocarpine-treated animals, synaptophysin immunolabeling was punctiform. Scale bars = 200 μm in A,C,E,G; 50 μm in B,D,F,H.

DISCUSSION

Acidic calponin is associated with neuroplastic changes observed in pilocarpine-treated rats

In the pilocarpine model of temporal lobe epilepsy, we report a striking increase in acidic calponin in the inner one-third molecular layer of the DG, the region of intensive network reorganization. These increased levels of acidic calponin occurred at 1 and 2 weeks after pilocarpine injection, when mossy fiber sprouting began to

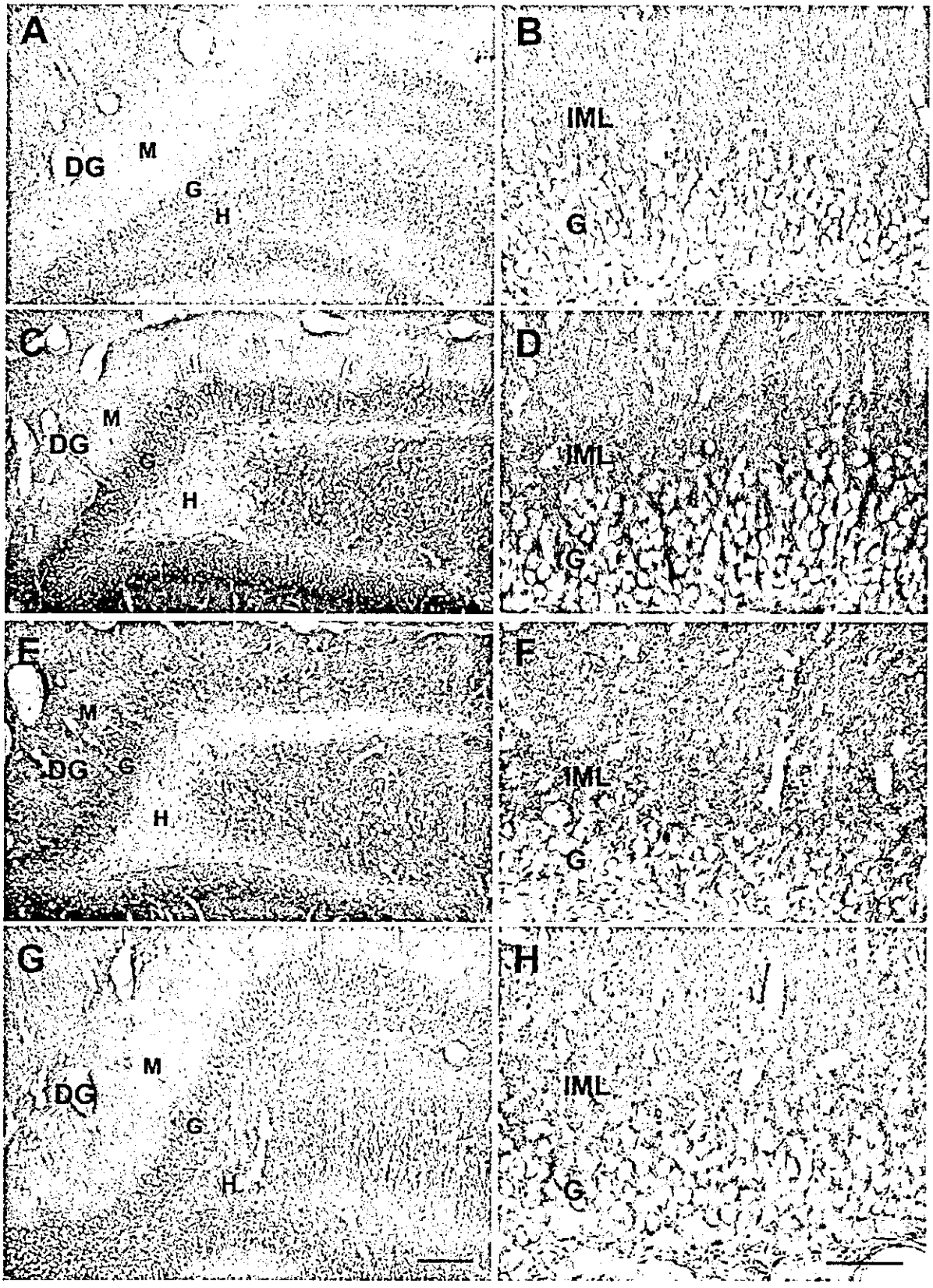

FIGURE 3.